ENGINEERING OF BIOMATERIALS

INŻYNIERIA BIOMATERIAŁÓW

JOURNAL OF POLISH SOCIETY FOR BIOMATERIALS AND FACULTY OF MATERIALS SCIENCE AND CERAMICS AGH-UST
CZASOPISMO POLSKIEGO STOWARZYSZENIA BIOMATERIAŁÓW I WYDZIAŁU INŻYNIERII MATERIAŁOWEJ I CERAMIKI AGH

Number 160
Numer 160
Volume XXIV
Rok XXIV

APRIL 2021
KWIECIEŃ 2021

ISSN 1429-7248

PUBLISHER:
WYDAWCA:

Polish Society for Biomaterials in Krakow
Polskie Stowarzyszenie Biomateriałów w Krakowie

ADDRESS OF EDITORIAL OFFICE:
ADRES REDAKCJI:

AGH-UST
30/A3, Mickiewicz Av.
30-059 Krakow, Poland
Akademia Górniczo-Hutnicza
al. Mickiewicza 30/A-3
30-059 Kraków

Issue: 250 copies
Nakład: 250 egz.

Scientific Publishing House AKAPIT
Wydawnictwo Naukowe AKAPIT
e-mail: wn@akapit.krakow.pl

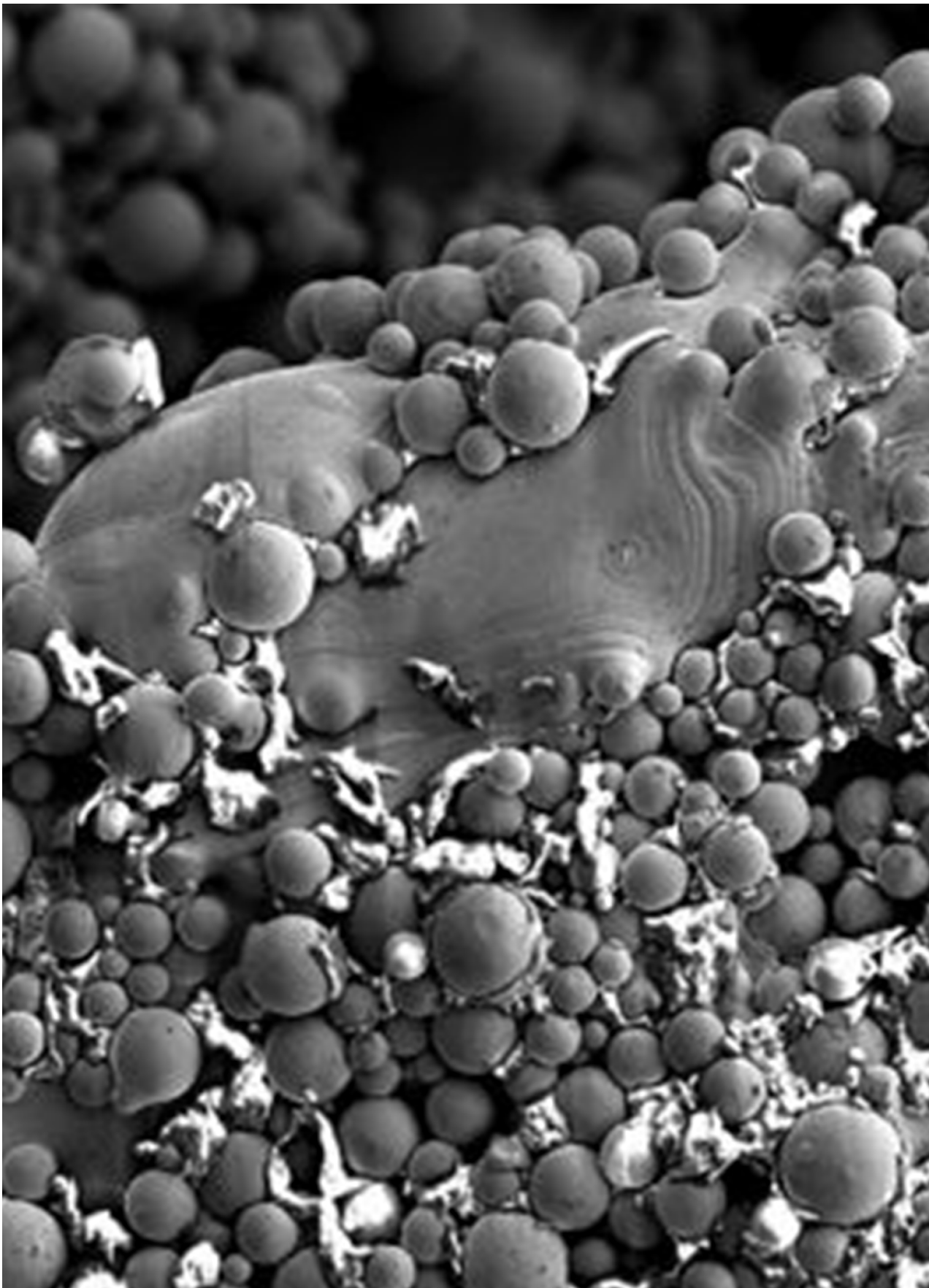

ENGINEERING OF
BIOMATERIALS

EDITORIAL BOARD
KOMITET REDAKCYJNY

INTERNATIONAL EDITORIAL BOARD
MIĘDZYNARODOWY KOMITET REDAKCYJNY

ENGINEERING OF BIOMATERIALS

Wskazówki dla autorów

1. Prace do opublikowania w kwartalniku „Engineering of Biomaterials / Inżynieria Biomateriałów" przyjmowane będą wyłącznie w języku angielskim.
2. Wszystkie nadsyłane artykuły są recenzowane.
3. Materiały do druku prosimy przysyłać za pomocą systemu online (www.biomaterials.pl).
4. Struktura artykułu:
• TYTUŁ • Autorzy i instytucje • Streszczenie (200-250 słów) • Słowa kluczowe (4-6) • Wprowadzenie • Materiały i metody • Wyniki i dyskusja • Wnioski • Podziękowania • Piśmiennictwo
5. Autorzy przesyłają pełną wersję artykułu, łącznie z ilustracjami, tabelami, podpisami i literaturą w jednym pliku. Artykuł w tej formie przesyłany jest do recenzentów. Dodatkowo autorzy proszeni są o przesłanie materiałów ilustracyjnych (rysunki, schematy, fotografie, wykresy) w oddzielnych plikach (format np. .jpg, .gif., .tiff, .bmp). Rozdzielczość rysunków min. 300 dpi. Wszystkie rysunki i wykresy powinny być czarno-białe lub w odcieniach szarości i ponumerowane cyframi arabskimi. W tekście należy umieścić odnośniki do rysunków i tabel.
6. Na końcu artykułu należy podać wykaz piśmiennictwa w kolejności cytowania w tekście i kolejno ponumerowany.
7. Redakcja zastrzega sobie prawo wprowadzenia do opracowań autorskich zmian terminologicznych, poprawek redakcyjnych, stylistycznych, w celu dostosowania artykułu do norm przyjętych w naszym czasopiśmie. Zmiany i uzupełnienia merytoryczne będą dokonywane w uzgodnieniu z autorem.
8. Opinia lub uwagi recenzentów będą przekazywane Autorowi do ustosunkowania się. Nie dostarczenie poprawionego artykułu w terminie oznacza rezygnację Autora z publikacji pracy w naszym czasopiśmie.
9. Za publikację artykułów redakcja nie płaci honorarium autorskiego.
10. Adres redakcji:

Czasopismo
„Engineering of Biomaterials / Inżynieria Biomateriałów"
Akademia Górniczo-Hutnicza im. St. Staszica
Wydział Inżynierii Materiałowej i Ceramiki
al. Mickiewicza 30/A-3, 30-059 Kraków
tel. (48) 12 617 44 48, 12 617 25 61
tel./fax: (48) 12 617 45 41
e-mail: epamula@agh.edu.pl, kabe@agh.edu.pl

Szczegółowe informacje dotyczące przygotowania manuskryptu oraz procedury recenzowania dostępne są na stronie internetowej czasopisma:
www.biomaterials.pl

Warunki prenumeraty

Zamówienie na prenumeratę prosimy przesyłać na adres:
mgr inż. Augustyn Powroźnik
apowroz@agh.edu.pl, tel/fax: (48) 12 617 45 41
Cena pojedynczego numeru wynosi 20 PLN
Konto: Polskie Stowarzyszenie Biomateriałów
30-059 Kraków, al. Mickiewicza 30/A-3
ING Bank Śląski S.A. O/Kraków
nr rachunku 63 1050 1445 1000 0012 0085 6001

Prenumerata obejmuje 4 numery regularne i nie obejmuje numeru specjalnego (materiały konferencyjne).

Instructions for authors

1. Papers for publication in quarterly journal „Engineering of Biomaterials / Inżynieria Biomateriałów" should be written in English.
2. All articles are reviewed.
3. Manuscripts should be submitted to editorial office through online submission system (www.biomaterials.pl).
4. A manuscript should be organized in the following order:
• TITLE • Authors and affiliations • Abstract (200-250 words) • Keywords (4-6) • Introduction • Materials and Methods • Results and Discussions • Conclusions • Acknowledgements • References
5. All illustrations, figures, tables, graphs etc. preferably in black and white or grey scale should be additionally sent as separate electronic files (format .jpg, .gif., .tiff, .bmp). High-resolution figures are required for publication, at least 300 dpi. All figures must be numbered in the order in which they appear in the paper and captioned below. They should be referenced in the text. The captions of all figures should be submitted on a separate sheet.
6. References should be listed at the end of the article. Number the references consecutively in the order in which they are first mentioned in the text.
7. The Editors reserve the right to improve manuscripts on grammar and style and to modify the manuscripts to fit in with the style of the journal. If extensive alterations are required, the manuscript will be returned to the authors for revision.
8. Opinion or notes of reviewers will be transferred to the author. If the corrected article will not be supplied on time, it means that the author has resigned from publication of work in our journal.
9. Editorial does not pay author honorarium for publication of article.
10. Address of editorial office:

Journal
„Engineering of Biomaterials / Inżynieria Biomateriałów"
AGH University of Science and Technology
Faculty of Materials Science and Ceramics
30/A-3, Mickiewicz Av., 30-059 Krakow, Poland
tel. (48) 12) 617 44 48, 12 617 25 61
tel./fax: (48) 12 617 45 41
e-mail: epamula@agh.edu.pl, kabe@agh.edu.pl

Detailed information concerning manuscript preparation and review process are available at the journal's website:
www.biomaterials.pl

Subscription terms

Contact:
MSc Augustyn Powroźnik,
e-mail: apowroz@agh.edu.pl
Subscription rates:
Cost of one number: 20 PLN
Payment should be made to:
Polish Society for Biomaterials
30/A3, Mickiewicz Av.
30-059 Krakow, Poland
ING Bank Slaski S.A.
account no. 63 1050 1445 1000 0012 0085 6001

Subscription includes 4 issues and does not include special issue (conference materials).

STUDIA PODYPLOMOWE

Biomateriały – Materiały dla Medycyny

2021/2022

Organizator: Akademia Górniczo-Hutnicza im. Stanisława Staszica w Krakowie Wydział Inżynierii Materiałowej i Ceramiki Katedra Biomateriałów i Kompozytów **Kierownik:** prof. dr hab. inż. Elżbieta Pamuła **Sekretarz:** dr inż. Małgorzata Krok-Borkowicz	**Adres:** 30-059 Kraków, Al. Mickiewicza 30 Pawilon A3, p. 208, 210 tel. 12 617 44 48, 12 617 23 38, fax. 12 617 33 71 email: epamula@agh.edu.pl; krok@agh.edu.pl https://www.agh.edu.pl/ksztalcenie/oferta-ksztalcenia/studia-podyplomowe-kursy-doksztalcajace-i-szkolenia/biomaterialy-materialy-dla-medycyny/

Charakterystyka:
Tematyka prezentowana w trakcie zajęć obejmuje przegląd wszystkich grup materiałów dla zastosowań medycznych: metalicznych, ceramicznych, polimerowych, węglowych i kompozytowych. Słuchacze zapoznają się z metodami projektowania i wytwarzania biomateriałów a następnie możliwościami analizy ich właściwości mechanicznych, właściwości fizykochemicznych (laboratoria z metod badań: elektronowa mikroskopia skaningowa, mikroskopia sił atomowych, spektroskopia w podczerwieni, badania energii powierzchniowej i zwilżalności) i właściwości biologicznych (badania: *in vitro* i *in vivo*). Omawiane są regulacje prawne i aspekty etyczne związane z badaniami na zwierzętach i badaniami klinicznymi (norma EU ISO 10993). Słuchacze zapoznają się z najnowszymi osiągnięciami w zakresie nowoczesnych nośników leków, medycyny regeneracyjnej i inżynierii tkankowej.

Sylwetka absolwenta:
Studia adresowane są do absolwentów uczelni technicznych (inżynieria materiałowa, technologia chemiczna), przyrodniczych (chemia, biologia, biotechnologia) a także medycznych, stomatologicznych, farmaceutycznych i weterynaryjnych, pragnących zdobyć, poszerzyć i ugruntować wiedzę z zakresu inżynierii biomateriałów i nowoczesnych materiałów dla medycyny. Słuchacze zdobywają i/lub pogłębiają wiedzę z zakresu inżynierii biomateriałów. Po zakończeniu studiów wykazują się znajomością budowy, właściwości i sposobu otrzymywania materiałów przeznaczonych dla medycyny. Potrafią analizować wyniki badań i przekładać je na zachowanie się biomateriału w warunkach żywego organizmu. Ponadto słuchacze wprowadzani są w zagadnienia dotyczące wymagań normowych, etycznych i prawnych niezbędnych do wprowadzenia nowego materiału na rynek. Ukończenie studiów pozwala na nabycie umiejętności przygotowywania wniosków do Komisji Etycznych i doboru metod badawczych w zakresie analizy biozgodności materiałów.

Zasady naboru:
Termin zgłoszeń: od 20.09.2021 do 20.10.2021 (liczba miejsc ograniczona - decyduje kolejność zgłoszeń)
Wymagane dokumenty: dyplom ukończenia szkoły wyższej
Osoby przyjmujące zgłoszenia:
prof. dr hab. inż. Elżbieta Pamuła (pawilon A3, p. 208, tel. 12 617 44 48, e-mail: epamula@agh.edu.pl)
dr inż. Małgorzata Krok-Borkowicz (pawilon A3, p. 210, tel. 12 617 23 38, e-mail: krok@agh.edu.pl)

Czas trwania: 2 semestry (od XI 2021 r. do VI 2022 r.) 8 zjazdów (soboty-niedziele) raz w miesiącu przewidywana liczba godzin: 160	**Opłaty:** 3 000 zł (za dwa semestry)

30th Biomaterials in Medicine and Veterinary Medicine

Anniversary Conference

14 – 17 October 2021 Rytro, Poland

SAVE THE DATE

14-17

OCTOBER

2021

www.biomat.agh.edu.pl

REGISTER

AND

SUBMIT

AN ABSTRACT

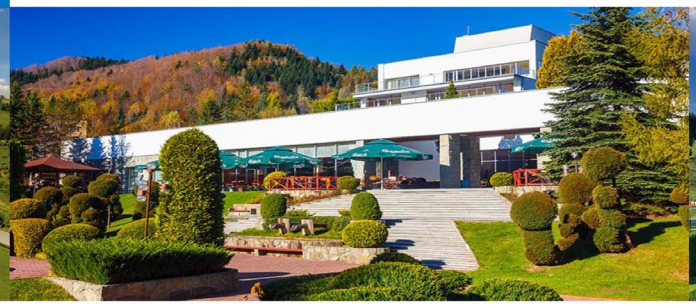

SPIS TREŚCI
CONTENTS

Wersja papierowa czasopisma „Engineering of Biomaterials / Inżynieria Biomateriałów" jest jego wersją pierwotną
Printed version of „Engineering of Biomaterials / Inżynieria Biomateriałów" is a primary version of the journal

BIOACTIVE CURDLAN/ AGAROSE DRESSING ENRICHED WITH GENTAMICIN FOR INFECTED WOUNDS – PILOT STUDIES

Michał Wójcik[1], Anna Wilczyńska[2], Vladyslav Vivcharenko[1], Paulina Kazimierczak[1], Łukasz Adaszek[2], Agata Przekora[1]*

[1] Independent Unit of Tissue Engineering and Regenerative Medicine, Chair of Biomedical Sciences, Medical University of Lublin, ul. W. Chodźki 1, 20-093 Lublin, Poland
[2] Department of Epizootiology and Clinic of Infectious Diseases, University of Life Sciences in Lublin, ul. Głęboka 30, 20-612 Lublin, Poland
*e-mail: agata.przekora@umlub.pl

Abstract

The problem of treating chronic wounds is widespread throughout the world and carries a huge cost. Biomaterials engineering tries to solve this problem by creating innovative bioactive dressings dedicated to specific types of wounds. Both synthetic and natural polymers are the main base to produce wound dressings. Biopolymers have the advantage over synthetic polymers by being more biocompatible, non-toxic, biodegradable, and eco-friendly. The aim of this work was to produce a bioactive biomaterial based on natural polymers with potential applications to manage chronic highly exuding and infected wounds. A newly developed method for chemical synthesis of the curdlan/agarose biomaterial at high temperature combined with freeze-drying process resulted in a superabsorbent dressing material with antibiotic immobilized. The obtained biomaterial was subjected to basic microbiological in vitro tests and a cytotoxicity assay according to ISO 10993-5. Moreover, the experimental treatment of the infected wound in a veterinary patient was performed using the developed material. Based on the conducted research, it was proved that the produced dressing is not toxic to normal human skin fibroblasts. An additional advantage of the biomaterial is its ability to inhibit the growth of harmful microorganisms, such as Staphylococcus aureus and Pseudomonas aeruginosa. Furthermore, the experimental treatment confirmed the validity of using the produced biomaterial as a dressing dedicated to the treatment of difficult-to-heal infected wounds. To summarize, the produced biomaterial possesses great potential to be used as a wound dressing for infected wounds.

Keywords: *biopolymers, wound dressing, cytotoxicity, antibacterial properties, wound healing*

[Engineering of Biomaterials 160 (2021) 2-7]

doi:10.34821/eng.biomat.160.2021.2-7

Introduction

Wound healing is a multistep process that can be divided into four distinct phases. In the case of skin damage, hemostasis occurs up to several hours after the injury. Then an inflammatory phase is activated and it lasts 1-3 days. The next stages are proliferation and repair which can last up to 4-21 days. The final step is remodelling taking up to a year [1,2]. Disruptions at any of these stages may delay wound healing and cause excessive scarring or chronic wound formation [2]. The main problem in the treatment of chronic wounds is an excess of exudate whose level does not decrease over time, comparing to wounds amenable to treatment [3]. In the case of chronic wounds, excessive exudate secretion is observed due to the active inflammatory process [4]. To limit the amount of exudate in the wound bed, an appropriate absorbent wound dressing is desired [5]. Dressings based on both synthetic and natural polymers are commonly used to treat chronic wounds. Synthetic polymers that are primarily used to produce wound dressings include poly(ethylene oxide) (PEO), polyglycolic acid (PGA), poly(vinyl pyrrolidone) (PVP), poly(ethylene glycol) (PEG), polylactide (PLA), polyurethane (PU), and poly(vinyl alcohol) (PVA). Biopolymers widely used for dressing materials involve alginate, agarose, cellulose, chitosan, collagen, dextran, and pectin [6]. Some natural polymers possess key features that have a positive effect on the healing process. For example, due to its natural antibacterial and pro-healing properties, chitosan is often used to accelerate wound healing and prevent infections in the wound bed [7].

It is well known, that chronic wounds provide the perfect environment to develop persistent infections. *Staphylococcus aureus*, *Klebsiella pneumoniae*, *Acinetobacter baumannii*, and *Pseudomonas aeruginosa* are the most common pathogens that hinder the healing process and cause significant tissue losses [8]. An additional problem is the ability of pathogenic bacteria (*Staphylococcus aureus* and *Pseudomonas aeruginosa*) to form a biofilm where the cells exhibit higher resistance to antibiotics than planktonic cells [9,10]. Incorporating antibiotics into the wound dressing structure is not recommended for the topical/local treatment of bacterial colonization in chronic wounds (bacteria are present but they do not elicit an immune response). The local antibiotic treatment may result in resistant bacterial strains, limited healing, or in extreme cases, a delayed hypersensitivity reaction. However, topical antibiotic therapy is required in the case of critical colonization or a serious bacterial infection [11]. Therefore, dressings containing embedded antibiotics are only used to treat infected and difficult-to-heal wounds.

A dressing for the treatment of chronic wounds should absorb and remove excessive exudate from the wound bed while providing an optimal moist environment. It should also be flexible and easily adaptable to the shape of the injury. At the same time it ought to cover the wound bed, providing mechanical protection against transmission of microorganisms. A wound dressing should tightly adhere to the wound bed but resist the skin cells adhesion so that changing the applied dressing will not destroy the newly formed tissue [11,12]. Hydrogel and hydrocolloid dressing materials appear to be the ideal candidates to manage chronic wounds as they address all of these criteria. Recently, the incorporation of bioactive compounds into the biomaterial structure has become a promising trend in regenerative medicine. Modern nanocomposite polymer-based hydrogel dressings for infected wounds are often enhanced with antibacterial nanoparticles and are widely studied nowadays [13,14].

The latest scientific reports describe successful new hydrogels loaded with gentamicin [15-17]. Gentamicin is an aminoglycoside antibiotic with outstanding thermal stability [16] which is commonly used to treat chronic and post-operational infections [18,19]. It is widely applied against infections caused by strains like aerobic Gram-negative bacteria and some aerobic Gram-positive bacteria [17]. The antibiotic exhibits a therapeutic serum level of 4-8 µg/ml and a toxic level of 12 µg/ml [19]. Rs indicate that the topical gentamicin treatment significantly increases clinical efficacy and reduces the wound healing time [20].

The aim of this study was to incorporate gentamicin within the structure of the previously developed foam-like curdlan/agarose biomaterial [21] to obtain a wound dressing for highly exuding and infected wounds. The developed curdlan/agarose wound dressing demonstrated to be non-toxic, biodegradable, and endowed with a high exudate absorption capacity. Moreover, the biomaterial did not allow for fibroblast adhesion, which is a desired phenomenon enabling the painless dressing removal after the healing process [21]. In this study, the gentamicin-enriched biomaterial was subjected to the cytotoxicity test using human skin fibroblasts and the antimicrobial activity evaluation against common bacteria causing wound infections. Moreover, the experimental treatment of an infected chronic wound in a veterinary patient was performed to confirm the clinical usefulness of the tested dressing.

Materials and Methods

Materials

The curdlan powder was obtained from Wako Pure Chemicals Industries. The agarose powder (gel point 36 ± 1.5°C), sodium dodecyl sulphate (SDS), gentamicin sulphate, phosphate-buffered saline (PBS), Eagle's Minimum Essential Medium (EMEM), penicillin, streptomycin, trypsin-EDTA, Thiazolyl Blue Tetrazolium Bromide (MTT) were purchased from Merck. The Mueller Hinton broth (MH) was obtained from Thermo Scientific. The fetal bovine serum was supplied from Pan-Biotech. Normal human skin fibroblast cell line (BJ), *Staphylococcus aureus* ATCC 25923, *Pseudomonas aeruginosa* ATCC 27853 were purchased from American Type Culture Collections (ATCC).

Preparation of the biomaterial

The biomaterial was prepared based on the method described in Polish Patent no. 236367 (2021). A foam-like biomaterial was prepared by mixing a predetermined amount of curdlan (2% w/v), agarose (2% w/v), and gentamicin sulphate (0.2% w/v) in deionized water. Thus, the concentration of gentamicin sulphate in the polymer suspension before gelation equalled 2 mg/ml. The combined suspension of polymers and antibiotic was preheated to 50°C on a magnetic stirrer. After a homogeneous mass was obtained, it was transferred to a mould and incubated in a water bath (20 min, 95°C). The produced samples were subjected to cooling, freezing, and finally lyophilization process. As a result, the foam-like biomaterial was obtained.

In vitro cell experiments

The *in vitro* cell viability experiment was carried out using human normal skin fibroblasts (BJ cell line). The cytotoxicity test and preparation of the extract were performed according to ISO 10993-5 standard [22]. BJ cells were seeded into a 96-multiwell plate using EMEM medium at the density of 2 x 10^4 cells/well and cultured for 24 h. Then, the culture medium was replaced with 100 µl of 100% extract of the material (prepared by placing 25 mg sample in 1 ml of the culture medium, followed by 24 h incubation at 37°C) and BJ cells were exposed to the extract for 48 h and 72 h. For control samples, the fresh EMEM medium was used instead of the extract. Next, the incubation media were removed and 100 µl of 1 mg/ml MTT solution was added per well. The plate was incubated with reagent at 37°C for 180 min. Afterwards, the 0.01% (w/v) SDS solution prepared in 0.01 M hydrochloric acid was added to degrade cells, release and solve formazan crystals. The cell viability was calculated by measuring the absorbance at 570 nm and was shown as a percentage of viability compared to the control (cells incubated in the EMEM medium instead of the biomaterial extract).

Inhibition of bacterial growth test

The antibacterial activity of the tested biomaterial was evaluated using the biomaterial extract prepared according to ISO 10993-5 in Mueller-Hinton (MH) broth. After incubation at 37°C for 24 h, the biomaterial extract was transferred into a 96-multiwell plate and then bacterium suspensions of 1.5 x10^5 CFU/ml of *S. aureus* ATCC 25923 and *P. aeruginosa* ATCC 27853 were added and incubated at 37°C for 48 h and 78 h. The growth control was performed from fresh MH broth and treated as above. Afterward, the cultures absorbance was measured at 660 nm and calculated as a percent of growth control.

Experimental treatment of a veterinary patient – case presentation

The owner with a fancy 2-year-old rat (*Rattus norvegicus domestica*), an uncastrated male with an abscess on the left side of the chest came to the Division of Small Mammals at the Department of Epizootiology and Clinics of Infectious Diseases of University of Life Sciences in Lublin (Poland). The change was already large with the focus on softening. The abscess was surgically cleaned and its cavity was rinsed with a 1% povidone iodine solution (Betadine, 100 mg/ml, EGIS). The antibiotic therapy with amoxicillin with clavulanic acid (Synulox 50 mg, Zoetis) at a dose of 20 mg/kg bodyweight twice a day was also advised. After the 3-week antimicrobial therapy, a small cavity, which was the residue of an abscess, remained in the skin. Due to severe itching caused by the wound healing, the animal was treated with Hydroxyzine (Hydroxyzinum VP, 2 mg/ml, Bausch Health) at a dose of 1 mg/kg bodyweight twice a day. The wound was also washed with 0.1% Rivanol solution. However, as the performed standard treatment was unsuccessful, the owner was offered the alternative treatment with the gentamicin-enriched hydrocolloid dressing. The wound was surgically cleaned and the gentamicin-loaded curdlan/agarose dressing was sewn into the abscess cavity. The experimental treatment was performed after obtaining written consent from the pet owner.

Statistical analysis

The cytotoxicity and antibacterial activity tests were performed in at least three distinct and independent repetitions. The obtained results were presented as the mean values ± standard deviations. The statistical analysis was performed with GraphPad Prism 8.0.1 Software with unpaired t-test ($p < 0.05$, a significance level of $\alpha = 0.05$).

Results and Discussions

The previously developed curdlan/agarose biomaterial (Polish Patent no. 236367) was modified by incorporating gentamicin during the production stage. The stiff foam-like biomaterial with a smooth surface was obtained via the high-temperature gelation of curdlan/agarose/gentamicin mixture followed by freezing and freeze-drying (FIG. 1a). The sample cross-section image shows the macroporous structure which should ensure good absorption, retention of fluids and adequate gas exchange (FIG. 1b). In the dry state, the dressing was characterized by a spongy structure. However, after its immersion into a fluid, it transformed to a soft gel able to adhere easily to the wound bed, thus acting like a typical hydrocolloid dressing. It should be mentioned that to our best knowledge there are only a few studies describing curdlan as a base for wound dressing production. The researchers created the curdlan-based hydrogel dressing by gelating the alkaline curdlan solution in a copper chloride. Nevertheless, the resultant biomaterial revealed high cytotoxicity against human skin cells [23]. In other studies, the silver-loaded nanofibrous curdlan was produced to manage difficult-to-treat wounds. Our research team reported superabsorbent foam-like dressings made of the curdlan/agarose mixture and the curdlan/chitosan blend that proved to have great potential for the treatment of highly exuding wounds [21].

Biocompatibility, non-toxicity, and biodegradability of the material are some of the main requirements for modern wound dressings [24]. To verify the cytotoxicity of the produced material, the MTT assay according to ISO 10993-5 standard was performed. The test results proved that the developed biomaterial containing gentamicin was non-toxic to BJ fibroblasts. The cell viability was equal to 80.5% and 83.5% after the 48 h and 72 h exposure of the cells to the biomaterial extract, respectively (FIG. 2). It should be noted that non-toxicity of gentamicin towards fibroblasts was also confirmed by other authors. For instance, Kilinç et al. proved non-toxicity of gentamicin at doses of 0.5-1 g/ml against L929 mouse fibroblast cells [25], whereas Hwang et al. demonstrated that the gentamicin-loaded PVA-dextran hydrogel had antibacterial properties, was non-toxic, and improved wound healing [17]. These research outcomes may indicate that the developed gentamicin-loaded curdlan/agarose biomaterial may have a beneficial effect on the healing process of infected wounds.

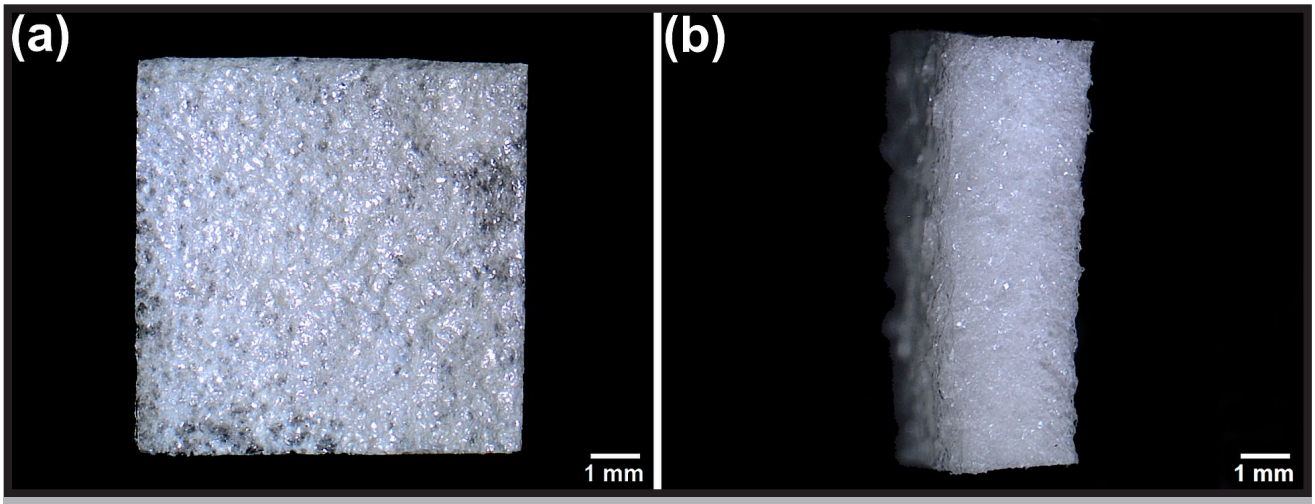

FIG. 1. Stereoscopic microscope (Olympus SZ61TR) images of the obtained biomaterial: (a) surface; (b) cross-section.

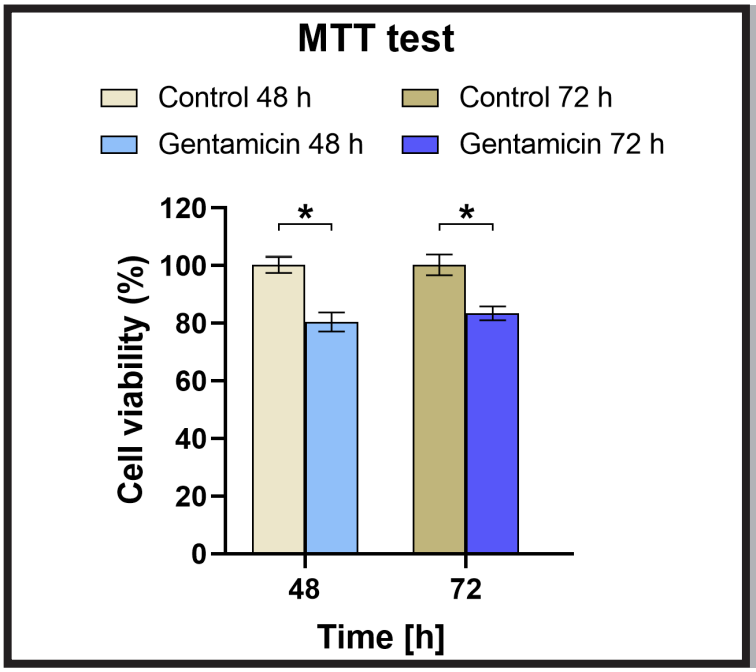

FIG. 2. Cytotoxicity of the gentamicin-enriched curdlan/agarose dressing against BJ fibroblasts evaluated by MTT assay with the 24-h extract of the biomaterial (the control – cells grown in the culture medium instead of the extract); * statistically significant results compared to the control (unpaired t-test).

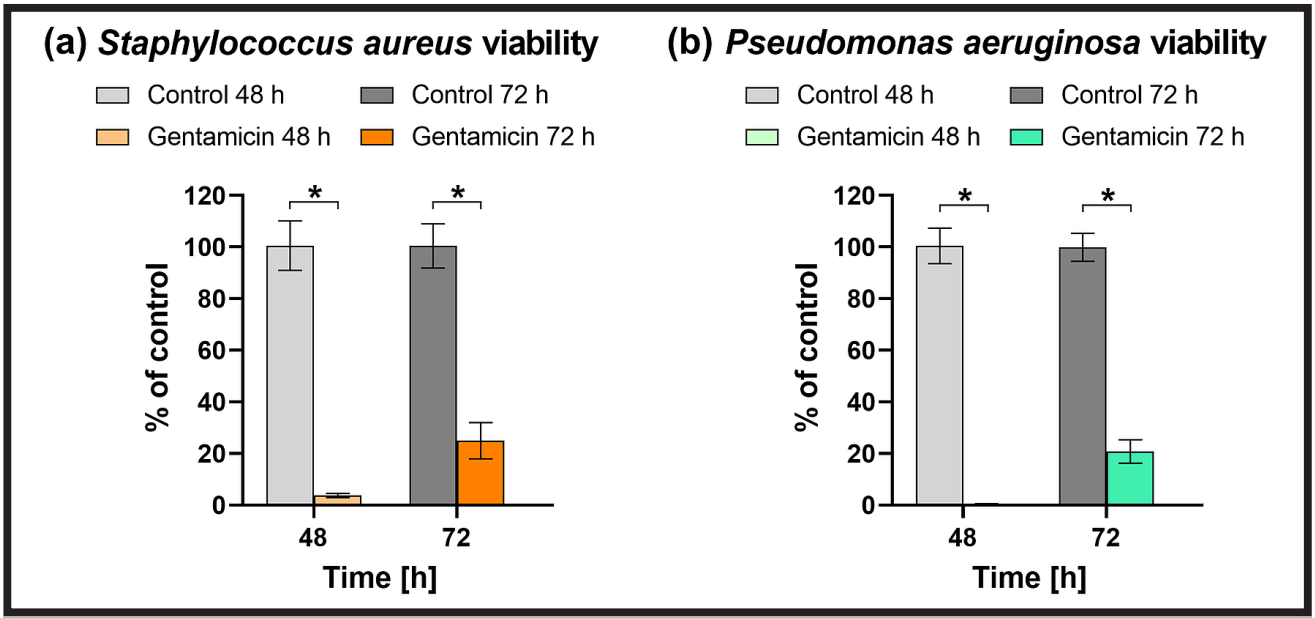

FIG. 3. Bacterial cell viability (as % of the control): (a) *Staphylococcus aureus* ATCC 25923 and (b) *Pseudomonas aeruginosa* ATCC 27853, after the 48 h and 72 h exposure to the biomaterial extract (prepared by 24 h incubation in the MH broth; the control – bacteria cultured in the MH broth instead of the extract); * statistically significant results compared to the control (unpaired t-test).

Scientific reports indicate that bacterial growth is a major contributor to chronic wounds. For this reason, wound dressings should reduce the microorganisms burden without cytotoxic effect against skin cells [26]. Our microbiological study proved that the tested biomaterial extract inhibited the bacterial growth both after two and three days of the experiment. In the case of *S. aureus*, the bacteria viability was equal to 3.8% and 25% after the 48 h and 72 h exposure time, respectively (FIG. 3a). Similarly, the *P. aeruginosa* viability was only 0.4% after 48 h and it increased to 20.8% after 72 h, compared to the control (FIG. 3b). Importantly, both bacterial strains strongly inhibited bacterial growth only after 48 h, as compared to the control. Thus, it may be assumed that gentamicin lost its therapeutic effectiveness during the 72 h incubation in the bacteria suspensions. It also indicates the necessity to change the wound dressing every 2 days during the treatment. The obtained results are in agreement with the reports presented by other authors who confirmed high effectiveness of gentamicin against bacterial strains related to wound infections. Studies of Tam et al. proved different profiles of antibacterial effect of gentamicin against *S. aureus* and *P. aeruginosa* [27]. It was also proven in a porcine model that gentamicin at a concentration of 2 mg/ml reduced *S. aureus* counts in the infected wounds [28].

The obtained here results indicate the great potential of the gentamicin-loaded biomaterial for infected wounds since the developed wound dressing exhibited antibacterial properties and non-toxicity against human skin cells. Based on the promising *in vitro* cell culture and microbiological tests, a decision to implement this biomaterial in the treatment of the veterinary patient was made.

Experimental treatment of a veterinary patient

Prior to the experimental treatment with the newly developed dressing material, the fancy rat was subjected to the standard treatment. However, the wound remained open and was oozing serous-purulent discharge, indicating secondary infection (FIG. 4a). Due to the unsuccessful standard treatment, the owner was offered a topical antibiotic therapy with the gentamicin-loaded curdlan/agarose dressing. To avoid the biomaterial damage by the scratching animal, the dressing was sewn into the abscess cavity. Immediately after the procedure, the normal healing process was observed. After 7 days of treatment, the dressing fell off along with the scab. The healed skin did not reveal any signs of infection (FIG. 4b). After 10 days, the reepithelialization process was almost completed (FIG. 4c), whereas on the 14th day the remaining scab fell off and the skin healing process was fully completed (FIG. 4d).

It should be noted that effective antibiotic release into the wound area is important to treat the infection [25]. Within this study, it was demonstrated that the 24-hour extract of the biomaterial had sufficient antibacterial activity *in vitro*. The antibacterial effectiveness of the dressing was also confirmed during the treatment of the veterinary patient. The advantage of the produced biomaterial was associated with its topical application to the infected wound. During contact with the exudate, the antibiotic was released from the dressing structure, reaching a therapeutic concentration that was not achievable with the systemic treatment. It is worth mentioning that by incorporating gentamicin within the curdaln/agarose biomaterial, it is possible to achieve the optimal drug accumulation tailored to the specific type and condition of the infected wound. To produce the optimal gentamicin-loaded dressing for infected wounds, it is planned to furtherly optimize the biomaterial gentamicin content to determine the antibiotic release profile.

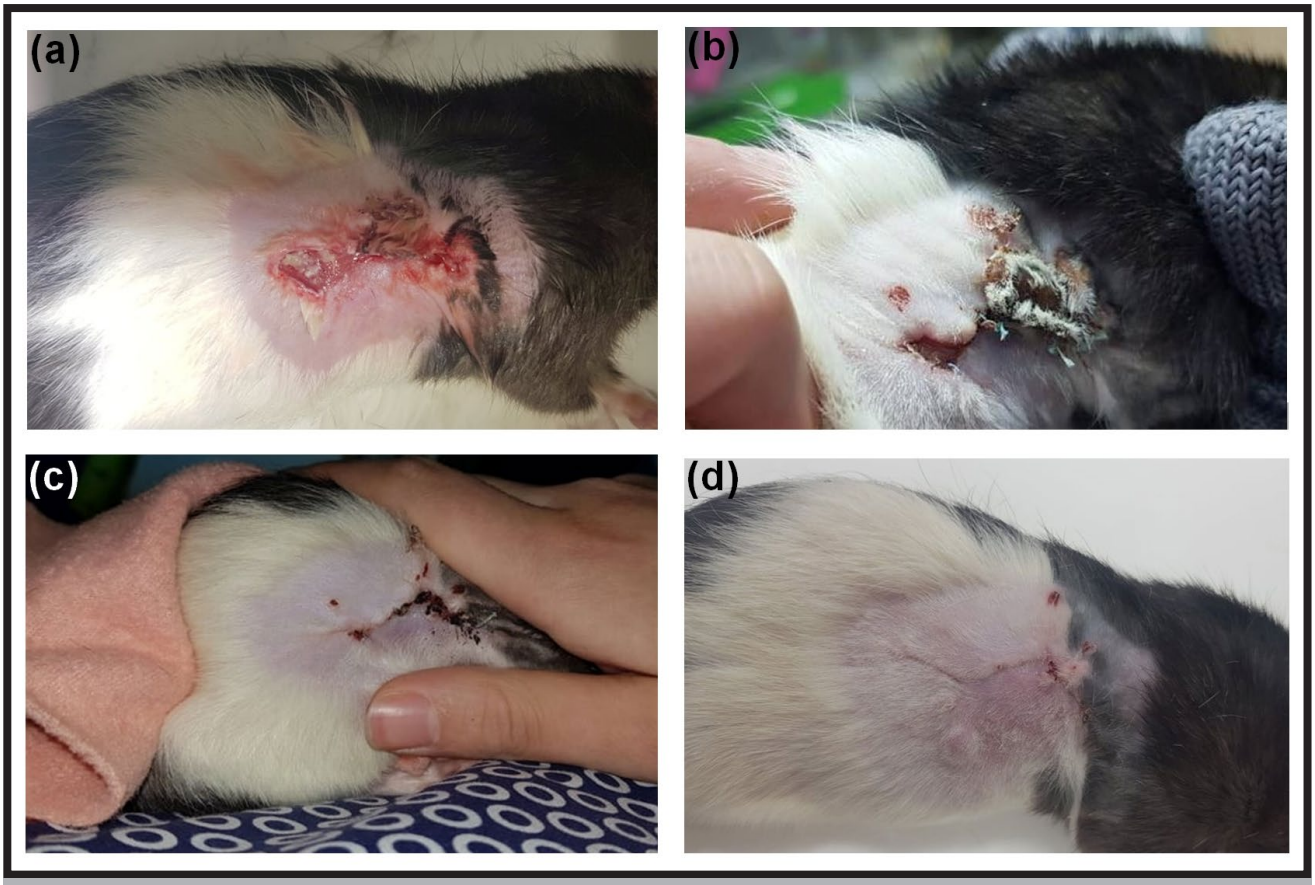

FIG. 4. Images of the wound area and its regeneration in a veterinary patient (*Rattus norvegicus domestica*): (a) before applying the dressing material, (b) the wound after 7 days, (c) the wound after 10 days, (d) the wound after 14 days.

Conclusions

The studies presented the production and basic characterization of the antibacterial hydrocolloid dressing material composed entirely of natural polymers (curdlan and agarose). The biomaterial contained a bioactive compound (i.e. gentamicin) that was loaded into its structure during the production stage. The conducted research proved that the biomaterial was not-toxic to normal human skin fibroblasts and exhibited the antibacterial activity against *S. aureus* and *P. aeruginosa* strains. Moreover, the presented clinical case proved that the gentamicin-loaded curdlan/agarose dressing applied as a drain for the local treatment of the infected wound significantly reduced the bacterial growth and accelerated the wound healing process. The biomaterial also limited the granulation tissue development and excessive scarring. The obtained results are promising, however, it is necessary to conduct further studies in order to confirm the applicability of developed biomaterial as a dressing used in the management of infected chronic wounds.

Acknowledgments

The research was funded by National Science Centre (NCN) in Poland within OPUS 16 grant no. UMO-2018/31/B/ST8/00945. The research was partially supported by the Ministry of Education and Science in Poland within the statutory activity of Medical University of Lublin (DS3/2021 project). Experimental treatment of the veterinary patient was financed within 'Innovation Incubator 4.0' programme (Measure 4.4 of the Smart Growth Operational Programme 2014-2020).

ORCID iDs

M. Wójcik: https://orcid.org/0000-0002-1918-6912
A. Wilczyńska: https://orcid.org/0000-0002-1148-6515
V. Vivcharenko: https://orcid.org/0000-0002-1526-686X
P. Kazimierczak: https://orcid.org/0000-0002-5893-7168
Ł. Adaszek: https://orcid.org/0000-0003-0261-2695
A. Przekora: https://orcid.org/0000-0002-6076-1309

References

[1] Ellis S., Lin E. J., Tartar D.: Immunology of wound healing. Current Dermatology Reports 7 (2018) 350–358.
[2] Landén N. X., Li D., Ståhle M.: Transition from inflammation to proliferation: a critical step during wound healing. Cellular and Molecular Life Sciences 73 (2016) 3861–3885.
[3] Moore Z., Strapp H.: Managing the problem of excess exudate. British Journal of Nursing 24 (2015) Sup15. S12.
[4] Przekora A.: A Concise review on tissue engineered artificial skin grafts for chronic wound treatment: Can we reconstruct functional skin tissue *in vitro*? Cells 9 (2020) 1–29.
[5] Walker A., Brace J.: A multipurpose dressing: Role of a hydrofiber foam dressing in managing wound exudate. Journal of Wound Care 28 (2019) S4–S10.
[6] Alven S., Aderibigbe B. A.: Chitosan and cellulose-based hydrogels for wound management. International Journal of Molecular Sciences 21 (2020) 1–30.
[7] Matica M. A., Aachmann F.I., Tøndervik A., et al.: Chitosan as a wound dressing starting material: Antimicrobial properties and mode of action. International Journal of Molecular Sciences 20 (2019) 1–33.
[8] Moghadam M., Khoshbayan A., Chegini Z., et al.: Bacteriophages, a new therapeutic solution for inhibiting multidrug-resistant bacteria causing wound infection: Lesson from animal models and clinical trials. Drug Design, Development and Therapy 14 (2020) 1867–1883.
[9] Chaney S. B., Ganesh, K., Mathew-Steiner S., et al.: Histopathological comparisons of *Staphylococcus aureus* and *Pseudomonas aeruginosa* experimental infected porcine burn wounds. Wound Repair and Regeneration 25 (2017) 541-549.
[10] Serra R., Grande R., Butrico L., et al.: Chronic wound infections: the role of *Pseudomonas aeruginosa* and *Staphylococcus aureus*. Expert Review of Anti-Infective Therapy 13 (2015) 605–613.
[11] Atkin L. Chronic wounds: the challenges of appropriate management. British Journal of Community Nursing 24 (2019) S26–S32.
[12] Vivcharenko V., Wojcik M., Przekora A.: Cellular response to vitamin C-enriched chitosan/agarose film with potential application as artificial skin substitute for chronic wound treatment, Cells 9 (2020) 1185.
[13] Li S., Dong S., Xu W., et al.: Antibacterial Hydrogels. Advanced Science 5 (2018) 1700527.
[14] Yang K., Han Q., ChenB., et al.: Antimicrobial hydrogels: Promising materials for medical application International Journal of Nanomedicine 13 (2018) 2217–2263.
[15] Dorati R., De Trizio A., Genta I., et al.: Gentamicin-loaded thermosetting hydrogel and moldable composite scaffold: Formulation study and biologic evaluation. Journal of Pharmaceutical Sciences: 106 (2017) 1596–1607.
[16] Kondaveeti S., De Assis Bueno P. V., Carmona-Ribeiro A. M., et al.: Microbicidal gentamicin-alginate hydrogels. Carbohydrate Polymers 186 (2018) 159-167.
[17] Hwang M. R., Kim J.O., Lee J. H., et al.: Gentamicin-loaded wound dressing with polyvinyl alcohol/dextran hydrogel: Gel characterization and *in vivo* healing evaluation. AAPS PharmSciTech 11 (2010) 1092–1103.
[18] Yetim I., Özkan O. V., Dervişoglu A., et al.: Effect of local gentamicin application on healing and wound infection in patients with modified radical mastectomy: A prospective randomized study. Journal of International Medical Research 38 (2010) 1442–1447.
[19] Varga M., Sixta B., Bem R., et al.: Application of gentamicin-collagen sponge shortened wound healing time after minor amputations in diabetic patients - A prospective, randomised trial. Archives of Medical Science 10 (2014) 283–287.
[20] Wang P., Long Z., Yu Z., et al.: The efficacy of topical gentamycin application on prophylaxis and treatment of wound infection: A systematic review and meta-analysis. International Journal of Clinical Practice 73 (2019) 1–11.
[21] Wojcik M., Kazimierczak P., Benko A., et al.: Superabsorbent curdlan-based foam dressings with typical hydrocolloids properties for highly exuding wound management. Materials Science and Engineering C 124 (2021) 112068.
[22] ISO 10993-5, Biological evaluation of medical devices - part 5: tests for in vitro cytotoxicity, The International Organization for Standardization (2009) 1–11.
[23] Nurzynska A., Klimek K., Swierzycka I., et al.: Porous curdlan-based hydrogels modified with copper ions as potential dressings for prevention and management of bacterial wound infection - An *in vitro* assessment. Polymers 12 (2020) 8–10.
[24] Ghomi E. R., Khalili S., Khorasani S. N., et al.: Wound dressings: Current advances and future directions. Journal of Applied Polymer Science 136 (2019) 1–12.
[25] Kilinç S., Tunç T., Pazarci Ö., et al.: Research into biocompatibility and cytotoxicity of daptomycin, gentamicin, vancomycin and teicoplanin antibiotics at common doses added to bone cement. Joint Diseases and Related Surgery 31 (2020) 328–334.
[26] Dabiri G., Damstetter E., Phillips T.: Choosing a wound dressing based on common wound characteristics. Advances in Wound Care 5 (2016) 32–41.
[27] Tam V. H., Kabbara S., Vo G., et al.: Comparative pharmacodynamics of gentamicin against *Staphylococcus aureus* and *Pseudomonas aeruginosa*. Antimicrobial Agents and Chemotherapy 50 (2006) 2626–2631.
[28] Junker J. P. E., Lee C. C. Y., Samaan S., et al.: Topical delivery of ultrahigh concentrations of gentamicin is highly effective in reducing bacterial levels in infected porcine full-thickness wounds. Plastic and Reconstructive Surgery 135 (2015) 151–159.

POST-PROCESSING OF TITANIUM 3D PRINTOUTS WITH RADIO FREQUENCY PLASMA

Jacek Grabarczyk[1], Krzysztof Jastrzębski[1]*, Maciej Wrotniak[2]

[1] Institute of Materials Science and Engineering, Lodz University of Technology, Stefanowskiego 1/15, 90-924 Lodz, Poland
[2] Clinical Department of Orthopedic-Traumatic, Oncological and Reconstructive Surgery, St. Barbara Specialized Regional Hospital No. 5, Sosnowiec, Plac Medyków 1, 41-200 Sosnowiec, Poland
*e-mail: Krzysztof.Jastrzebski@p.lodz.pl

Abstract

Additive manufacturing is a technology of great interest for biomedical engineering and medicine since it enables to mimic natural structures. The 3D printouts require post-processing to ensure desired surface properties and interaction with living matter. The presented research focuses on novel approaches involving plasma treatment of Ti6Al4V scaffolds obtained by Direct Metal Printing. Solid samples and scaffolds of two various geometries were treated in atmospheres of pure argon, argon and oxygen or pure oxygen. The effect of post-processing was evaluated with scanning electron microscopy, measurements of mass, and surface roughness.

In all the examined cases the proposed post-processing method reduces the amount of loosely bonded powder particles remaining after printing. The changes of mass before and after the treatment are much lower than in the case of popular wet chemical methods. The character of undergoing post-processing depends on the process atmosphere resulting in physical etching or the combination of physical etching and chemical oxidation. The action of argon or argon/oxygen plasma reduces mass to the level of only 1% while by use of pure oxygen atmosphere even the slight increase of the overall sample mass is observed.

The plasma etching was successfully introduced for the treatment of titanium 3D printouts to minimize the detachment of powder particles. That method not only is much softer than chemical etching but it can also lead to specific surface structurization that may be beneficial regarding medical applications of such printouts.

Keywords: *post-processing, plasma treatment, 3D printing, titanium printouts, RF plasma*

[Engineering of Biomaterials 160 (2021) 8-14]

doi:10.34821/eng.biomat.160.2021.8-14

Introduction

Additive manufacturing is of great interest to scientific teams from around the world and from various industries [1]. That collective name applies to a group of methods resulting in three-dimensional elements by application of successive layers of material – i.e. 3D printing. This approach enables manufacturing of low-quantity series of products, or even individual personalized details, almost regardless of the complexity of their shape. 3D printing techniques are of great interest, especially regarding applications in biomedical engineering or medicine [2-4].

Currently, it is possible to control the size and distribution of implant pores [5,6], which has a significant impact on the processes of the implant/body integration by inducing angiogenesis and the mammalian cells growth [7]. Nevertheless, the structure of human and animal tissues is characterized by a complex architecture, often a hierarchical structure with complex porosity [8,9], the reconstruction of which goes beyond the scope of conventional design and manufacturing approaches. However, 3D printing techniques give more freedom to develop new structures for such specific applications requiring mimicry of nature.

An important aspect of 3D printing for potential biomedical applications is the use of additional surface treatments that can modify its porosity, change the surface energy, and influence the biological response [10]. Technologies based on powder sintering may leave residues on the both the elements surface and in the pores which are not integrated with any constituent. Therefore, in the case of medicine and biomedicine living tissues, it is necessary to remove such residues to prevent their uncontrolled release to the surrounding environment. Currently, the post-processing of metal prints involves mechanical methods [11], such as shaking, blowing, shot blasting, and those related with chemical treatment, such as baths in acid solutions [12,13] or electrochemical treatment [14,15]. The new approach to post-processing of 3D prints may involve their plasma etching. So far, such an approach is rather used for polymers [16] or modification of the metal powders [17] and not the metal prints themselves.

It should be remembered that the element subjected to post-processing to remove unbound powder residues undergo significant changes that highly affect its main properties. The main effect is smoothening of the scaffold. Wu et al. [14] reached over the 5-time improvement in the level of Ra between the untreated and the chemically polished 3D titanium prints. These changes can improve biological response [18], but also reduce mechanical properties [19] or even cause the loss of material integrity, especially due to single struts thinning [20]. Wysocki et al. [13] showed that only 3 minutes of chemical polishing with the mixture of HF and HNO_3 can lead to an over 50% mass reduction of the treated scaffold.

The following article is focused on the description of the novel approach to post-processing of metal 3D prints. The investigations were conducted on the Ti6Al4V scaffolds prepared by means of DMP (Direct Metal Printing) method so as to determine the effectiveness of plasma-ion treatment of such elements in order to eliminate defects and impurities remaining after the printing process.

Materials and Methods

Samples preparation

The tested samples were cylinders – 16 mm in diameter and 5 mm of height, prepared by means of ProX DMP 320 printer. The laser power was 500 W, the layer thickness ranged from 30 to 60 microns and the accuracy of the printout was ± 0.2%. The printing material was the Ti6Al4V ELI alloy available under the trade name LaserForm® Ti Gr23 (A).

Samples of variable filling resulting in different geometry of obtained scaffolds were analyzed within this study. FIG. 1 presents images of the examined 3D printouts: 100% infill (no intentional voids were left during printing either on the surface or inside the sample), scaffolds with beams oriented at right or variable angles (denoted respectively solid, geo1, and geo2).

Post-processing

The plasma-ion post-processing was carried with radio frequency etching. Modified samples were placed in the vacuum chamber directly on the electrode. Three types of the working atmosphere were analyzed: argon (99.999% purity), oxygen (99.999% purity) and the mixture of argon and oxygen. The working pressure was 15 Pa for the usage of single gas and 20 Pa double gases. In all the cases the flow rate of each used gas was set for 8 sccm. The etching was conducted under the negative potential bias of 2200 V. The temperature of the modified elements was 500°C. The duration of the post-processing was constant in all the analyzed cases and equalled 4 h. The list of used parameters and the designation of the type of modification is presented in TABLE 1.

Scanning electron microscopy (SEM)

The SEM investigation was used to visualize and evaluate the topography of all the examined samples. SM-6610LV (JEOL, USA) equipped with X-Max 80 energy dispersive X-ray spectroscopy (EDS) analyzer (Oxford Instruments, UK) was used for observations with secondary imaging mode (SEI – secondary electron image) – acquiring topographic images. The SEM observations at randomly selected spots were carried out under high vacuum with an electron beam acceleration voltage of 10-20 kV.

Mass control

Five samples of each type of the examined printouts (solid, geo1, and geo2) were used to determine the impact of the proposed post-processing method on the mass change. For each sample, the measurements were conducted prior to plasma etching and after that process. The evaluation of mass variation was conducted with an Asix AGS60 moisture analyzer with a weight accuracy of 0.001 g. The samples were heated to 100°C and kept at that temperature until a constant mass of the sample was obtained for at least 60 s.

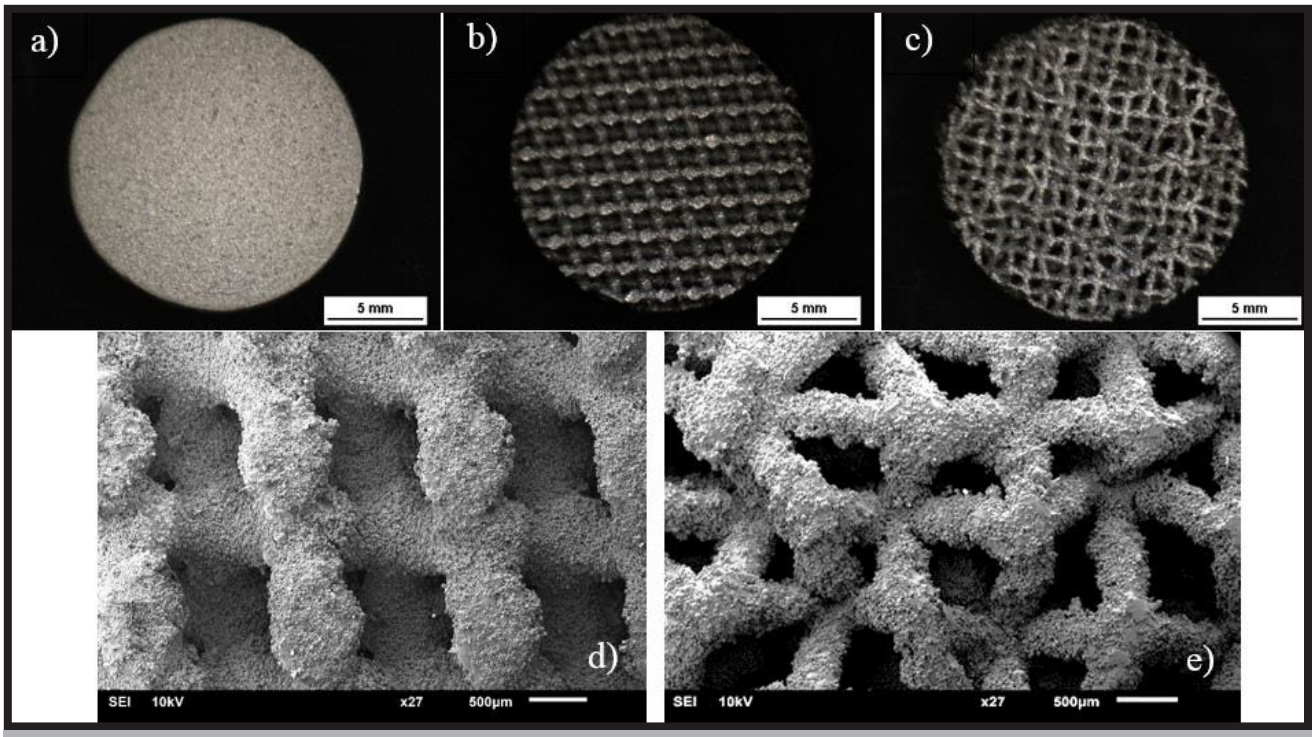

FIG. 1. Macroscopic images of analyzed samples: a) solid sample – 100% infill, b) geo1 – right angles beams, c) geo2 - individual beams crossing at variable angles; and SEM images of scaffolds d) geo1, e) geo2.

TABLE 1. Parameters of used plasma etching.

No.	Working gas	Potential [V]	Pressure [Pa]	Gas flow [sccm]	Temperature [°C]	Time [h]	Code of modification
1	Oxygen	-2200	15	8	500	4	O_2
2	Argon		15	8			Ar
3	Oxygen & Argon		20	8 (Ar) 8 (O_2)			Ar/O_2

Surface characterization

The evaluation of surface roughness was conducted via contact profilometry by means of Hommel Tester T1000. For each sample, 6 profiles were collected before and after post-processing. The values of the following parameters: Ra, Rz, Rmax were analyzed.

Results and Discussions

The roughness measurement carried out after plasma etching of solid samples (FIG. 2) revealed differences, in relation to the unmodified sample, only for the argon plasma. In this case, the Rz and Rmax parameters increased by about 20%. However, no significant differences were found for the O_2 and Ar/O_2 modification. Usually, post-processing reduces surface roughness. The results of chemical or electrochemical polishing presented by Pyka et al. [19] or Wu et al. [14] show a decrease of printouts roughness, respectively by up to 25% and even about 5 times (for Ra parameter). Also, other methods like jet-blasting show a similar tendency but with minor effects, e.g. the results of Kim et al. [16]. In that study, the areal surface roughness of scaffolds single struts changed from 11.0 ± 4.1 μm to 10.6 ± 3.8 μm after post-processing. The argon plasma resulting from the high negative potential of electrode autopolarization is related with a basically physical effect of surface etching - the predominant result is a spontaneous change in topography.

The incorporation of oxygen into the plasma atmosphere mitigates this effect. Oxidation takes place in addition to the physical etching of the surface. In the case of etching in pure oxygen, this effect is dominating, which results in a slight increase in the mass of samples after the modification. Such an effect is in opposition to the mass loss observed in other types of etching. The results of the EDS surface examination (FIG. 3) show that the highest oxygen content in the surface of the sample etched in oxygen plasma which reaches the level of about 40%, while for the sample modified in the mixture of argon and oxygen, this value is only about 25%. The least amount of oxygen is present in the case of samples etched in pure argon, only about 10%. When discussing the change in the sample mass values after the plasma etching process, it should be noted that the measured differences are small. They are in the range of 0.3-0.5% for the solid samples and 0.5-0.7% for the scaffolds (FIG. 4). This is a much better effect than in the case of chemical cleaning of 3D prints, where the weight loss can be up to several dozen percent [13].

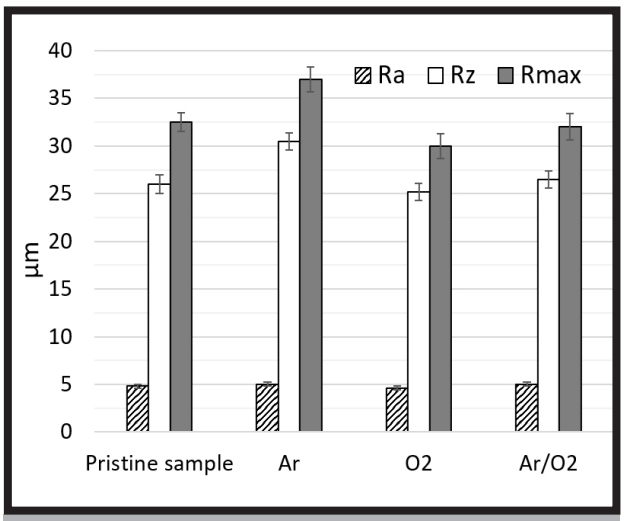

FIG. 2. Comparison of the roughness changes of pristine solid 3D printouts and those modified by plasma etching in various working atmospheres.

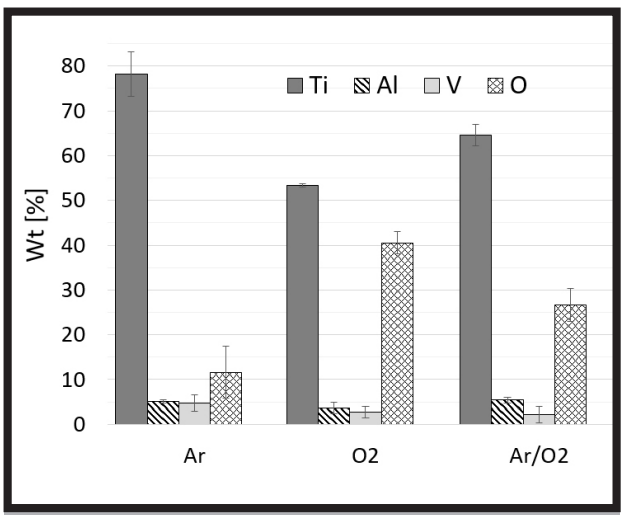

FIG. 3. Chemical composition of solid samples modified by plasma etching in various working atmospheres.

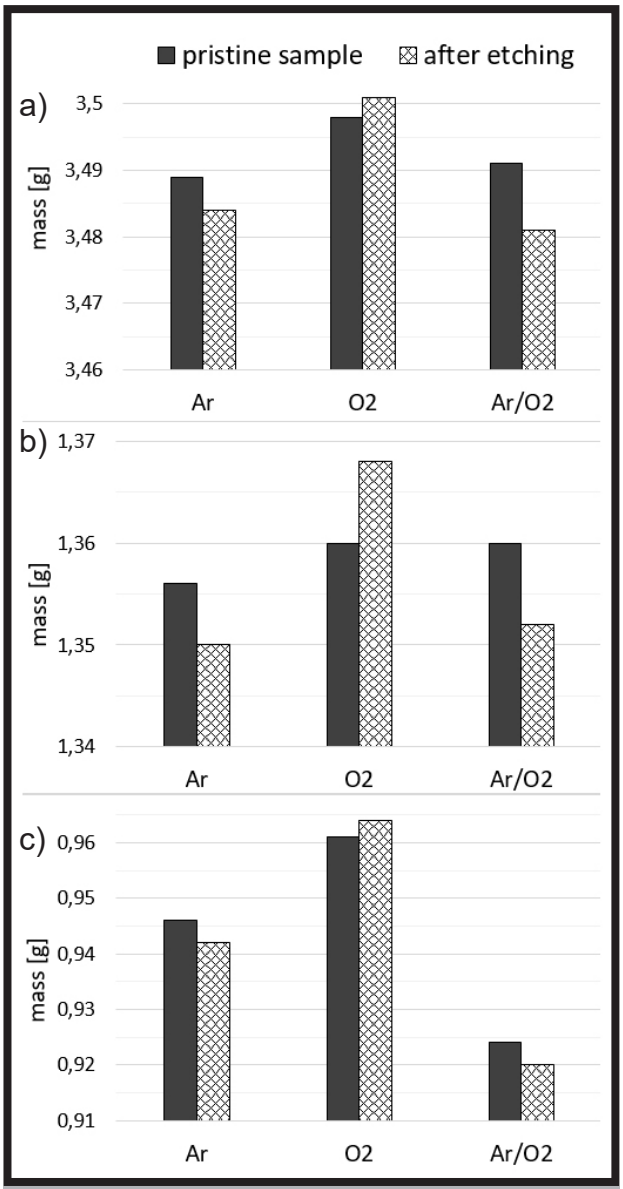

FIG. 4. Changes of mass of printouts modified by plasma etching in various working atmospheres. a) solid, b) geo1, c) geo2.

The SEM analysis of the plasma-treated solid samples showed high efficiency of that post-processing method in removing residual powders from the surface (FIG. 5). Regardless of the chemical composition of the reaction atmosphere, the etching effect is similar. Only a few residues of powders with a larger diameter, that are more tightly bound to the substrate, remained on the examined surfaces. Similar effects were achieved by other research groups working with standard methods of post-processing [12-14]. More loosen powder particles – contacting the substrate with only a small part of the surface, are completely removed. Higher magnifications (FIG. 6) reveal the differences in the effect of Ar and O_2/Ar modification. The argon plasma etching creates a specific microstructure on the sample surface. As a result, the increase of surface roughness appears, which was confirmed not only by the SEM images but also by profilometry (FIG. 2). Additionally, the structure defects remaining after the printing process, such as microcracks, are more visible, which may additionally contribute to increasing the roughness, especially the Rmax parameter. The oxygen plasma etching, especially in pure oxygen, results in significantly smoother surfaces of the printouts. This difference results from the previously discussed coexisting chemical oxidation and physical etching. This may also be favoured by the surface temperature during the plasma process, stabilizing at about 500°C. The oxidation effect also masks possible structure defects.

The etching effect is slightly different for treated scaffolds but looks similar in the case of both examined geometries of the printouts (FIGs 7 and 8). The cleaning, in this case, is not as effective as in the case of solid samples. Powder residues are visible on all surfaces. The weakest cleaning effect was obtained for the Ar/O_2 modification – minor, insignificant changes in the amount or geometry of residual powders. Usage of argon or pure oxygen plasma leads to the similar final state of the examined samples. In both cases, there are visible the remaining particles of used powders on the surface of scaffolds. What is more, the change in their geometry is clear – swap from round to more angular shape of individual particles. There are no observed powders whose contact surface with the substrate would be small enough to cause a risk of their easy detachment. Therefore, it can be concluded that the obtained effect of etching is satisfactory in these cases. A different etching effect for scaffolds and solid samples may be due to two reasons. The first is possibly scattering of the plasm in the subsurface area leading to decrease of the efficiency of the process, resulting from larger and more complicated geometries. Secondly, the structure of the scaffold printouts is uneven. It seems that there exist areas of beams that can be treated as solid and those where the powder has not been melted well enough, resulting in the formation of something like a porous sinter produced by the chaotic thermal fusion of a large group of powder particles. Due to the small size of the individual beams forming the overall structures, the attempt to completely remove such mentioned above porous structures would involve a significant reduction in their size, which in turn may lead to a weakening of the strength properties of the printout.

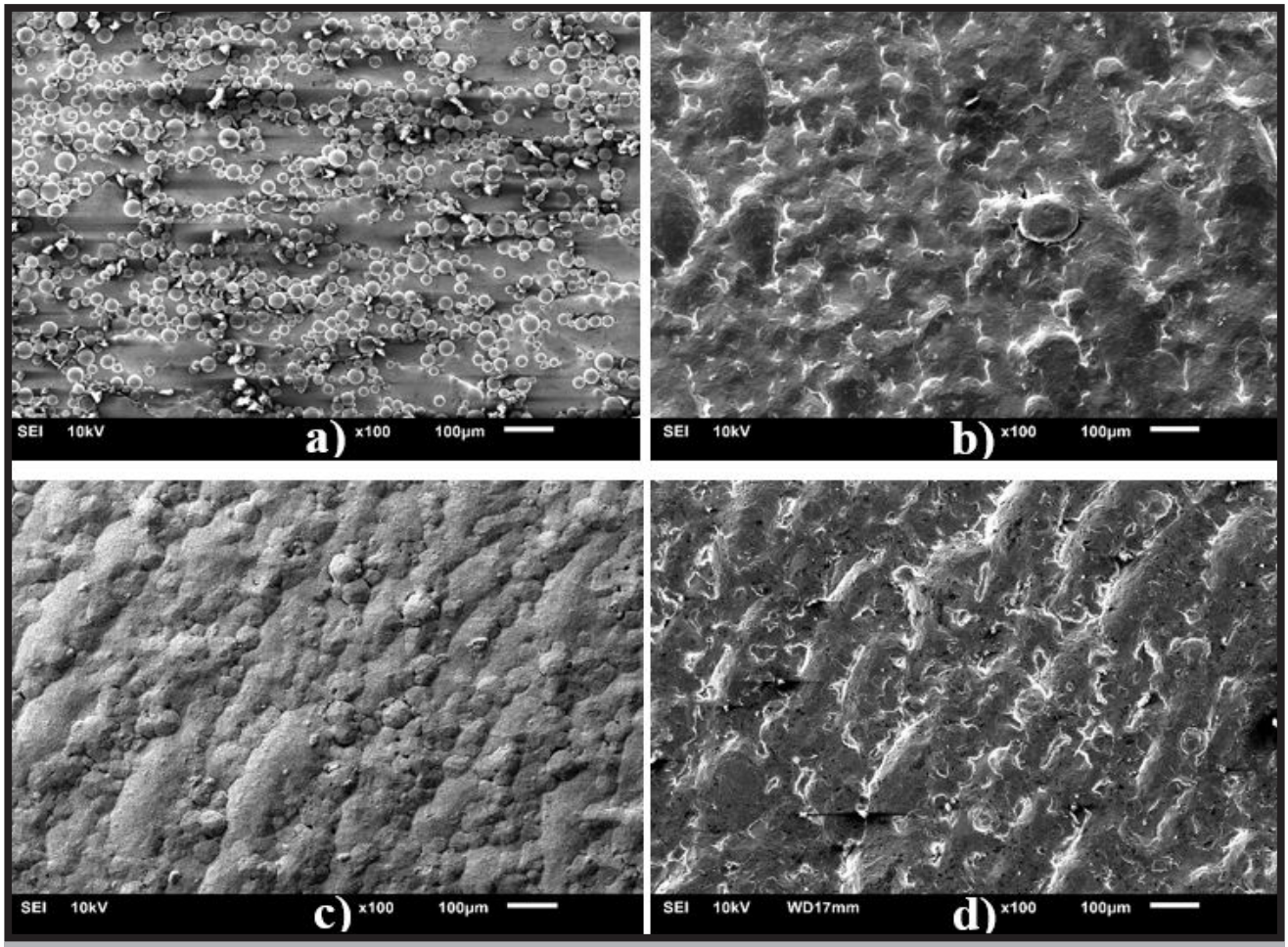

FIG. 5. SEM images of the surface of solid samples modified in various manners – 100x magnification. a) Pristine state, b) O_2 modification, c) Ar modification, d) Ar/O_2 modification.

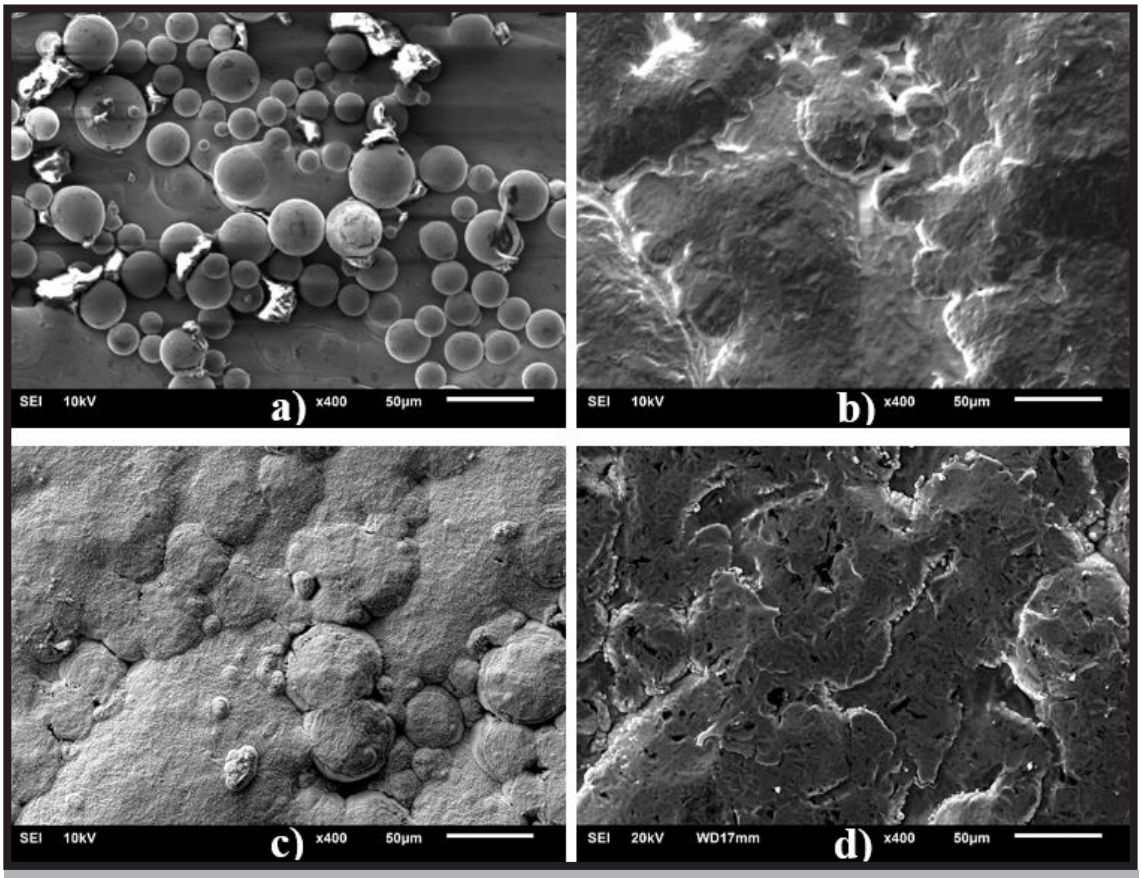

FIG. 6. SEM images of the surface of solid samples modified in various manners – 400x. a) Pristine state, b) O_2 modification, c) Ar modification, d) Ar/O_2 modification.

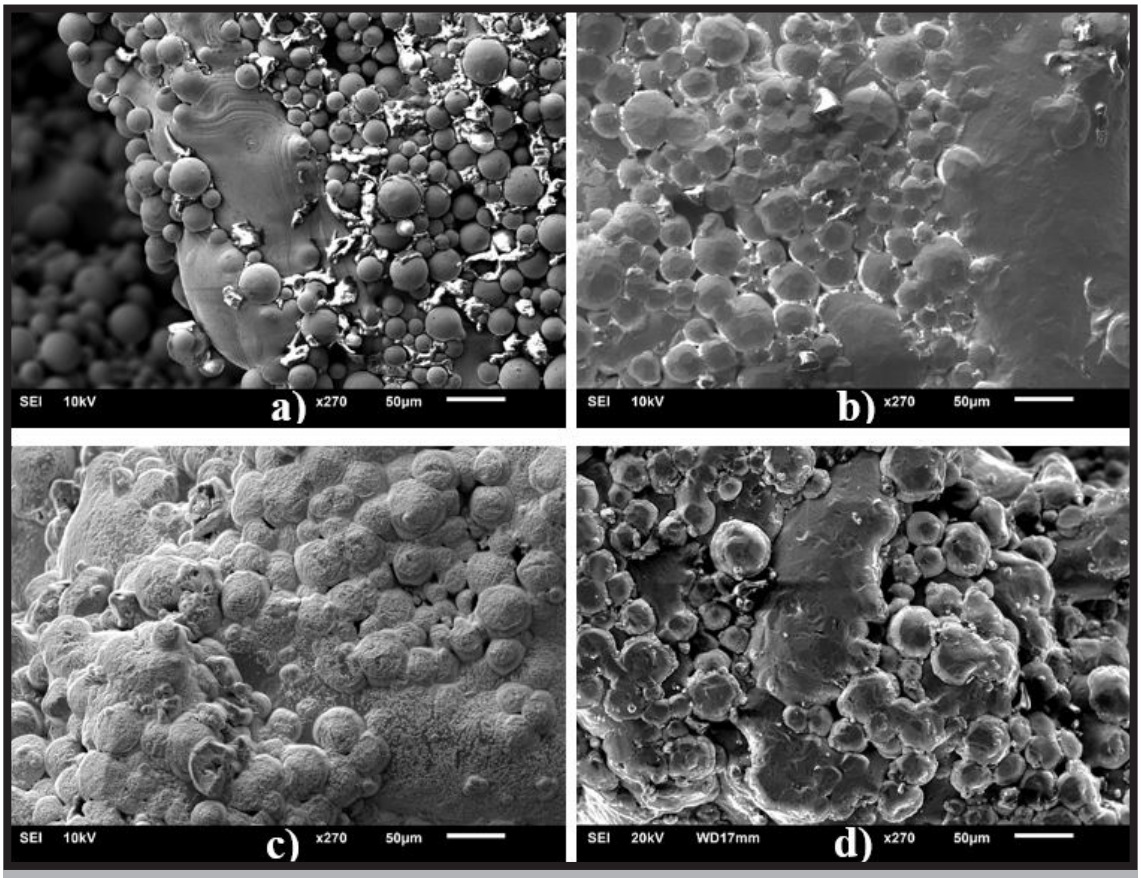

FIG. 7. SEM images of the surface of geo1 samples modified in various manners. a) Pristine state, b) O_2 modification, c) Ar modification, d) Ar/O_2 modification.

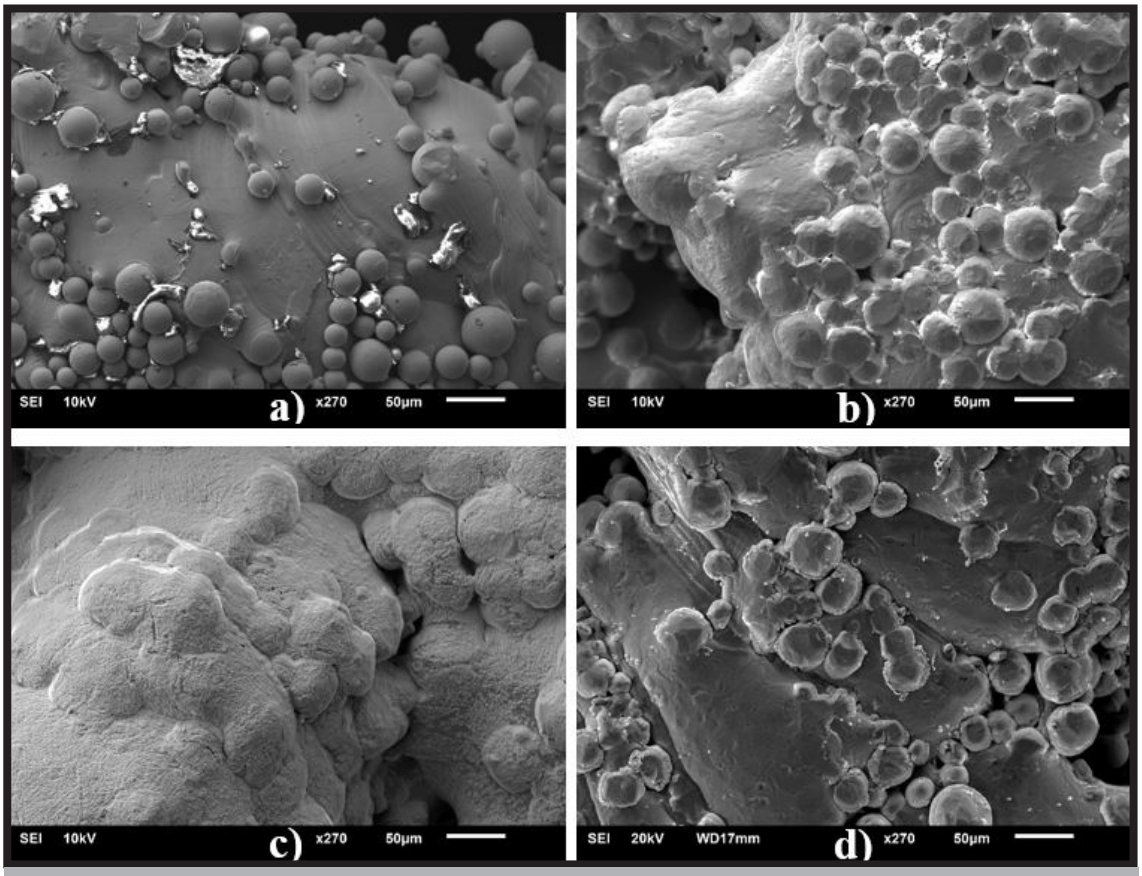

FIG. 8. SEM images of the surface of geo2 samples modified in various manners. a) Pristine state, b) O_2 modification, c) Ar modification, d) Ar/O_2 modification.

Conclusions

The presented results show that the plasma treatment of titanium elements obtained via the DMP method is a possible novel approach to the post-processing of 3D printouts which reduces loosely bonded remaining particles of the powders used during manufacturing. Depending on the applied kind of the working atmosphere, it is possible to conduct predominantly physical etching (action of Ar plasma) or a combination of physical etching and chemical oxidation (use of O_2, or Ar/O_2 plasma).

The proposed method is much less invasive than common chemical etching and results in the mass reduction of the examined printouts of less than 1% (for the usage of pure argon or its mixture with oxygen) or even a slight increase of that parameter due to the formation of the oxide layer. The proposed approach was more effective in cleaning loosely attached powder particles from elements with simpler geometry, but in all the examined cases the possible detachment of powders particles was effectively minimized.

The disadvantage of the plasma method may be its time-consuming nature. In the presented research, etching was carried out for up to 4 h, while in the currently most popular method of wet chemical etching, this process does not exceed several minutes. However, the increase in processing time can be compensated by the advantages. The first benefit is a small, even negligible loss of weight, important especially in scaffolds printouts as it does not change their strength properties. The second advantage is the obtained microstructure which can be related with more favourable conditions of the surface for cell adhesion.

Acknowledgements

This work was financed from the resources assigned to Internal grant from the fund of young researchers of the Faculty of Mechanical Engineering of the Lodz University of Technology entitled: „Porównanie wpływu metod postprocessingu na właściwości powierzchni elementów tytanowych uzyskiwanych technologią druku 3D".

ORCID iDs

J. Grabarczyk: https://orcid.org/0000-0003-0155-2432
K. Jastrzębski: https://orcid.org/0000-0001-7170-4257
M. Wrotniak: https://orcid.org/0000-0002-4329-8623

References

[1] Shahrubudin N., Lee T.C., Ramlan R.: An Overview on 3D Printing Technology Technological, Materials, and Applications. Procedia Manufacturing 35 (2019) 1286-1296.

[2] Gottsauner M., Reichert T., Koerdt S., Wieser S., Klingelhoeffer C., Kirschneck C., Hoffmann J., Ettl T., Ristow O.: Comparison of additive manufactured models of the mandible in accuracy and quality using six different 3D printing systems. Journal of Cranio--Maxillofacial Surgery (2021)

[3] Dumpa N., Butreddy A., Wang H., Komanduri N., Bandari S., Repka M.A.: 3D printing in personalized drug delivery: An overview of hot-melt extrusion-based fused deposition modeling. International Journal of Pharmaceutics 600 (2021) 120501.

[4] Guoqing Z., Junxin L., Chengguang Z., Juanjuan X., Xiaoyu Z., Anmin W.: Design Optimization and Manufacturing of Bio-fixed tibial implants using 3D printing technology. Journal of the Mechanical Behavior of Biomedical Materials 117 (2021) 104415.

[5] Novitskaya E., Hamed E., Li J., Manilay Z., Jusiak I., McKittrick J.: Hierarchical Structure of Porosity in Cortical and Trabecular Bones. MRS Online Proceedings Library 1420 (2012) 24-29.

[6] Sari M., Hening P., Chotimah, Ana I. D., Yusuf Y.: Porous structure of bioceramics carbonated hydroxyapatite-based honeycomb scaffold for bone tissue engineering. Materials Today Communications 26 (2021) 102135.

[7] Hollister S.J.: Porous scaffold design for tissue engineering. Nat Mater 5 (2005) 518-524.

[8] Torres Y., Trueba P., Pavón J.J., Chicardi E., Kamm P., García--Moreno F., Rodríguez-Ortiz J.A.: Design, processing and characterization of titanium with radial graded porosity for bone implants. Materials & Design 110 (2016) 179-187.

[9] Ahn T., Gidley D.W., Thornton A.W., Wong-Foy A.G, Orr B.G, Kozloff K.M., Banaszak Holl M.M.: Hierarchical Nature of Nanoscale Porosity in Bone Revealed by Positron Annihilation Lifetime Spectroscopy. ACS Nano 15 (2021) 4321-4334.

[10] Worts N., Jones J., Squier J.: Surface structure modification of additively manufactured titanium components via femtosecond laser micromachining. Optics Communications 430 (2019) 352-357.

[11] Kim T.B., Yue S., Zhang Z., Jones E., Jones J.R., Lee P.D.: Additive manufactured porous titanium structures: through-process quantification of pore and strut networks. J. Mater. Process. Technol. 214 (2014) 2706-2715.

[12] Łyczkowska E., Szymczyk P., Dybała B., Chlebus E.: Chemical polishing of scaffolds made of Ti–6Al–7Nb alloy by additive manufacturing Arch. Civ. Mech. Eng. 14 (2014) 586-594.

[13] Wysocki B., Idaszek J., Buhagiar J., Szlązak K., Brynk T., Kurzydłowski K.J., Święszkowski W.: The influence of chemical polishing of titanium scaffolds on their mechanical strength and in-vitro cell response. Materials Science and Engineering: C 95 (2019) 428-439.

[14] Wu Y.C., Kuo C.N., Chung Y.C., Ng C.H., Huang J.C.: Effects of Electropolishing on Mechanical Properties and Bio-Corrosion of Ti6Al4V Fabricated by Electron Beam Melting Additive Manufacturing. Materials 12 (2019) 1466.

[15] Urlea V., Brailovski V.: Electropolishing and electropolishing--related allowances for powder bed selectively laser-melted Ti-6Al-4V alloy components. Journal of Materials Processing Technology 242 (2017) 1-11.

[16] Kim J.Y., Kim W.J., Kim G.H.: Scaffold with micro/nanoscale topographical cues fabricated using E-field-assisted 3D printing combined with plasma-etching for enhancing myoblast alignment and differentiation. Applied Surface Science 509 (2020) 145404.

[17] Liu Z., Yang C., Chen T., Cai W.S., Liu L.H., Kang L.M., Wang Z., Li X.Q., Zhang W.W., Li Y.Y.: Influence of discharge plasma modification on physical properties and resultant densification mechanism of spherical titanium powder. Powder Technology 389 (2021) 138-144.

[18] Wysocki B., Idaszek J., Buhagiar J., Szlązak K., Brynka T., Kurzydłowski K.J., Święszkowski W.: The influence of chemical polishing of titanium scaffolds on their mechanical strength and in--vitro cell response. Materials Science & Engineering C 95 (2019) 428-439.

[19] Pyka G., Burakowski A., Kerckhofs G., Moesen M., Van Bael S., Schrooten J., Wavers M.: Surface Modification of Ti6Al4 V Open Porous structures Produced by additive manufacturing. Adv Eng Mater 14 (2012363-370).

[20] Chang S., Liu A., Yee C., Ong A., Zhang L., Huang X., Tan Y.H., Zhao L., Li L., Ding J.: Highly effective smoothening of 3D-printed metal structures via overpotential electrochemical polishing. Materials Research Letters 7 (2019) 282-289.

NEW MATERIALS BASED ON HYALURONIC ACID AND EGG ALBUMIN MIXTURE

Magdalena Gadomska*, Katarzyna Musiał, Alina Sionkowska

Department of Biomaterials and Cosmetics Chemistry,
Nicolaus Copernicus University in Torun,
Gagarin 7, 87-100 Torun, Poland
*e-mail: 291013@stud.umk.pl

Abstract

In this work, new materials based on the mixture of hyaluronic acid and albumin from chicken eggs have been studied. Tests were carried out to determine the molecular weight of the tested hyaluronic acids. The properties of hyaluronic acid were investigated and significant differences were found in the mechanical properties of the tested compound, depending on its molecular weight. It was found that egg albumin can be combined with hyaluronic acid and thin films can be obtained. Spectrometric tests were performed both for pure compounds and for mixtures of hyaluronic acid with chicken egg albumin. IR spectroscopy showed that interactions between hyaluronic acid and egg albumin are mainly by hydrogen bonds, as the shifts in the main bands in IR spectra were observed. The addition of egg albumin to hyaluronic acid leads to the decrease of its mechanical properties. The deterioration of the mechanical properties of polymer films from HA-albumin mixtures may be due to interactions between compounds which were shown in the IR spectra. The thin films based on hyaluronic acid and egg albumin blend can be used as adhesive materials in biomedicine and cosmetics. Both biopolymers are biocompatible and biodegradable so we can expect a biocompatible and biodegradable material for potential application as adhesives.

Keywords: *hyaluronic acid, albumin from chicken egg, mechanical properties, polymer films*

[Engineering of Biomaterials 160 (2021) 15-21]

doi:10.34821/eng.biomat.160.2021.15-21

Introduction

The definition of a biomaterial states that it is a chemically or pharmacologically inert substance intended for implantation or contact with a living organism. The biomaterial must meet several basic conditions. It must be non-toxic, biocompatible, and non-carcinogenic. It cannot react with a living organism causing unwanted reactions. Biomaterials can be divided into several basic groups: bioinert (any material that does not cause a negative response by the body's immune system), bioactive, and bioabsorbable [1]. Biomaterials are used in tissue engineering to create healing materials and also as drug delivery systems. Natural polymers, such as proteins, nucleic acids, polysaccharides, are most often used as scaffolds or substrates in biomaterials [2]. The new trend in materials sciences is the fabrication of new biomaterials based on the mixtures of biopolymers. Within the last three decades, an increasing interest in new materials based on blends of two or more polymers has been observed [3-9]. The potential applications of biopolymer blends in the biomedical field can be wide and may include drug delivery systems, tissue engineering, wound healing, or gene therapy. Biopolymer blends can be also applied as edible packaging materials.

Polysaccharides and their modifications have found wide application in the medical and pharmaceutical industries as drug carriers [10]. They may show anti-inflammatory, antiviral, and antibacterial properties, which makes them good raw materials for the production of biomedical materials. They can be of plant or animal origin. The most common natural polysaccharides are cellulose, starch, chitosan and hyaluronic acid [11]. The above-mentioned polysaccharides can be blended with another biopolymer. One of the most commonly used polysaccharides is hyaluronic acid (HA). HA is a water-soluble compound whose structure includes D-glucuronic acid and N-acetyl-d-glycosamine [12]. Hyaluronic acid has been used in ophthalmology, embryo protection, and drug delivery because it is a non-toxic, non-inflammatory, non-allergenic compound, as well as a highly elastic hydrophilic substance [1]. Hyaluronan is also used in eye drops because its sodium salt is present in the vitreous body of the human eye [13]. Hyaluronic acid can be blended with another polymer and/or a biopolymer and in this way, new materials can be obtained [14-20].

In the biomaterials industry, apart from polysaccharides, proteins occupy a special place due to their low cost, high availability, and biodegradability [21]. Proteins can also be considered as a component of the blend with polysaccharides. The most common types of albumin in the biomaterials industry are human albumin, bovine albumin, and egg albumin. Egg albumin is composed of glycoprotein and amino acid residues. Polymer films obtained from chicken egg white have the appropriate properties, thanks to which they can be used as food packaging material. Moreover, egg albumin is biocompatible and biodegradable [22]. It can be blended with water-soluble polysaccharides and in such a way new materials can be fabricated. Biopolymer blends preparation by dissolution in the same solvent allows avoiding protein denaturation. The specific interaction between the blend components is often called miscibility. The most common interactions in the blends are: hydrogen bonding (when polymers contain chemical groups capable of forming hydrogen bonds), ionic and dipole, pi-electrons and charge-transfer complexes. The interactions between HA and egg albumin can determine the properties of the blend. Moreover, the interactions between hyaluronic acid and albumin can be important from biomedical point of view because the mixture of hyaluronic acid and albumin can mimic the synovial fluid and it may influence the tribological properties of cartilage. The blends of hyaluronic acid and albumin can be used in drug delivery systems so it is crucial to know the physico-chemical properties of such blends.

In this work polymer thin films made of pure hyaluronic acid of three different molecular weights and their mixtures with egg albumin have been researched. The mechanical and physicochemical properties of the obtained membranes were investigated and compared. To the best of the authors' knowledge, there is very limited information about the structural features of hyaluronic acid-albumin molecular assemblies, including intermolecular interaction characteristics.

Materials and Methods

Materials

High-molecular-weight hyaluronic acid (HA), low-molecular-weight HA, and ultra-low-molecular HA were purchased from the cosmetic company (Prochowice, Poland). Albumin from chicken egg was purchased from Sigma-Aldrich (Merck Life Science, Poznań, Poland).

Preparation of solutions

To determine viscometric average molecular weights of HA, a stock solution of NaCl was prepared in which the three tested hyaluronic acids were dissolved. The following solutions were obtained: a solution 0.1% of high-molecular HA in NaCl, a 0.1% solution of low-molecular HA in NaCl, and a 1% solution of ultra-low-molecular HA in NaCl.

For the study of mechanical properties and FTIR analyses, thin films were manufactured using the 1.5% high-molecular HA, the 1.5% low-molecular HA, and the 2% ultra-low-molecular HA solutions which were prepared in water.

Determination of viscometric average molecular weights

The prepared stock solution of hyaluronic acid in NaCl was poured into the Ubbelohde viscometer (Ubbelohde viscometer is a standard glass device commercially available). Then, the time of the solution flow between the two marked places was measured several times. The stock solution was then diluted with successive portions of the NaCl solution and the flow times were measured each time. The measurements were performed for three different hyaluronic acids. The molecular weights of the tested hyaluronic acids were determined with the help of a computational program.

The molecular weight of HA used in this study was as follows:

$M_{HAhigh\text{-}molecular} = 8{,}434 \cdot 10^5$ (g/mol)
$M_{HAlow\text{-}molecular} = 6{,}327 \cdot 10^5$ (g/mol)
$M_{HAultra\text{-}low\text{-}molecular} = 3{,}445 \cdot 10^4$ (g/mol)

Preparation of polymer blends and films

Each of the three hyaluronic acid solutions was mixed with powdered egg albumin. The amount of 0.3 g powdered albumin was added to 30 g of HA solution and then stirred for about 15 min on a magnetic stirrer. Then 25 g of the resulting mixtures and the pure solutions of the three test HAs were poured onto plastic plates. It took a week for the solvent to evaporate and the polymer film to form. The images of the films obtained in such a way are shown in FIG. 1 and FIG. 2.

IR spectroscopy

The infrared spectra were registered by Nicolet iS10 spectrophotometer equipped with an ATR device with a germanium crystal (Thermo Fisher Scientific, Waltham, MA, USA). All the spectra were recorded with the resolution of 4 cm^{-1} with 64 scans. The spectra were evaluated in the range of 400-4000 cm^{-1}. The data was obtained using the Omnic Spectra 2009 program.

Mechanical properties

Fittings of the same size were cut from all the obtained polymer films. Mechanical properties, including tensile strength force and Young's modulus, were tested on a Zwick & Roell Z.0.5 testing machine (ZwickRoell Group, Ulm, Germany). 10 trials were made for each film. Initial parameters of the research program were as follows: initial force 0.1 MPa, initial force speed 5 mm/min, testing speed 50 mm/min, the load cell is 0.5 N. The data was collected in the testXpert II 2017 program. The statistical analysis of the obtained results was performed using the Q-Dixon test in MS Excel.

Results and Discussions

Physicochemical properties

The IR spectra were recorded to determine the interactions between hyaluronic acid and albumin. The individual spectra of pure compounds and mixtures are presented in the figures below (FIGs. 3-8). The positions of the individual bands are presented in the tables below (TABLES 1-3).

FIG. 1. Image of the film made from the 1.5% low molecular weight HA solution.

FIG. 2. Image of the film made from the mixture of 1.5% low molecular weight HA with egg albumin.

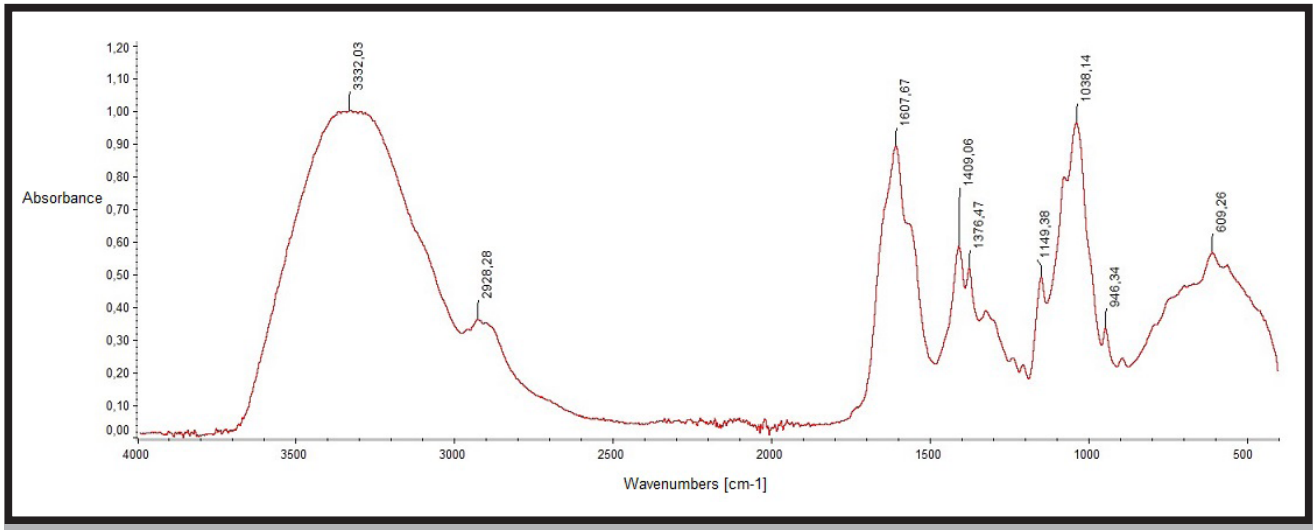

FIG. 3. IR spectrum of the 1.5% HA high molecular weight.

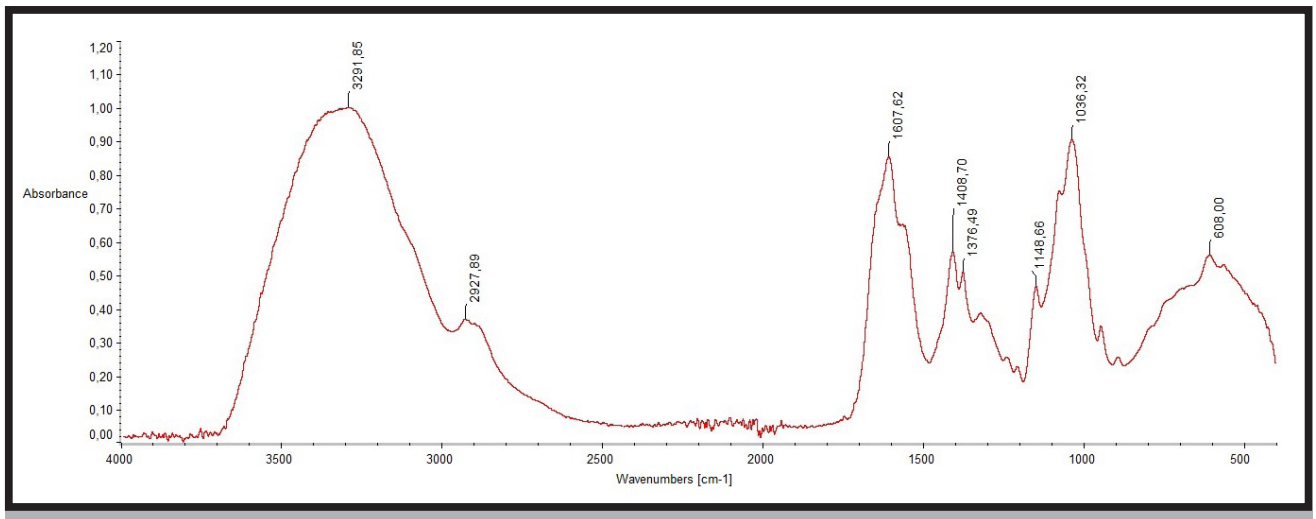

FIG. 4. IR spectrum of 1.5% HA low molecular weight.

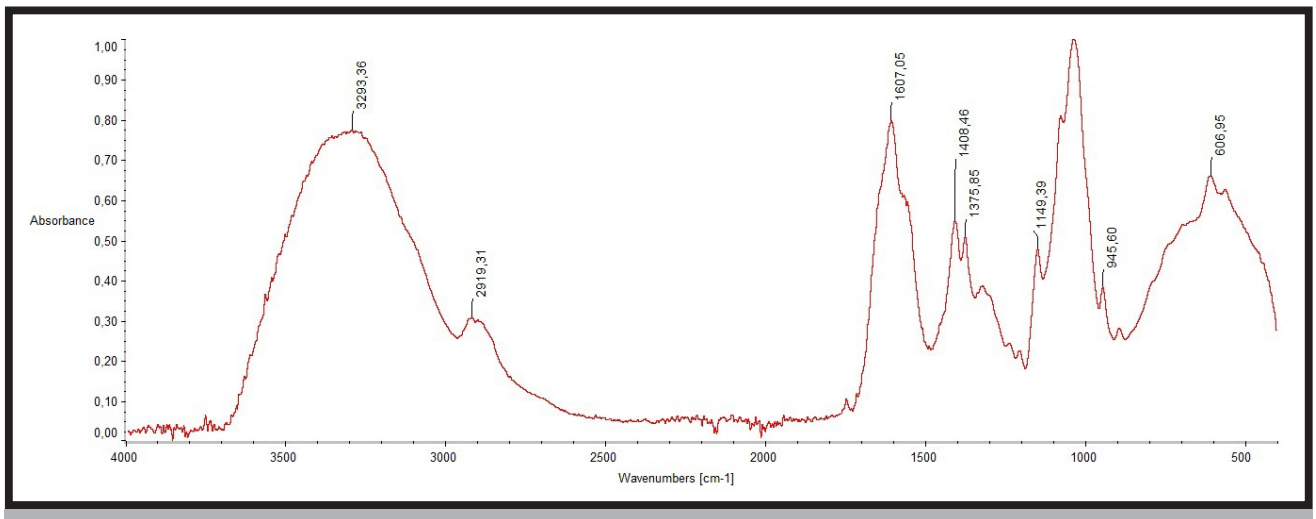

FIG. 5. IR spectrum of the 2% ultra-low molecular weight HA.

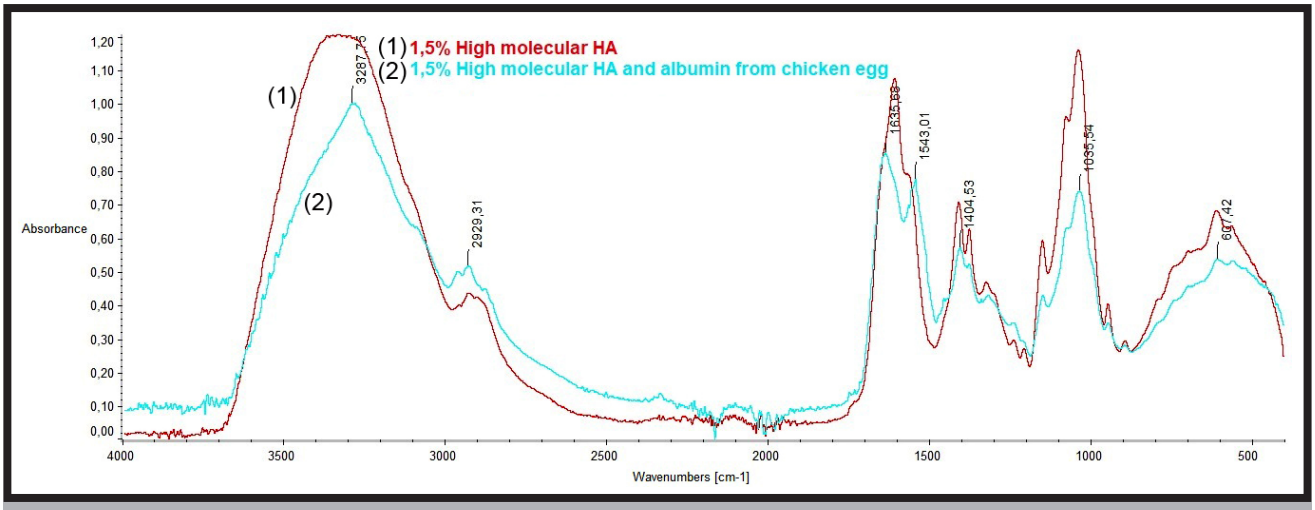

FIG. 6. IR spectrum of the mixture of 1.5% HA high molecular HA with albumin and IR spectrum of the pure high molecular HA.

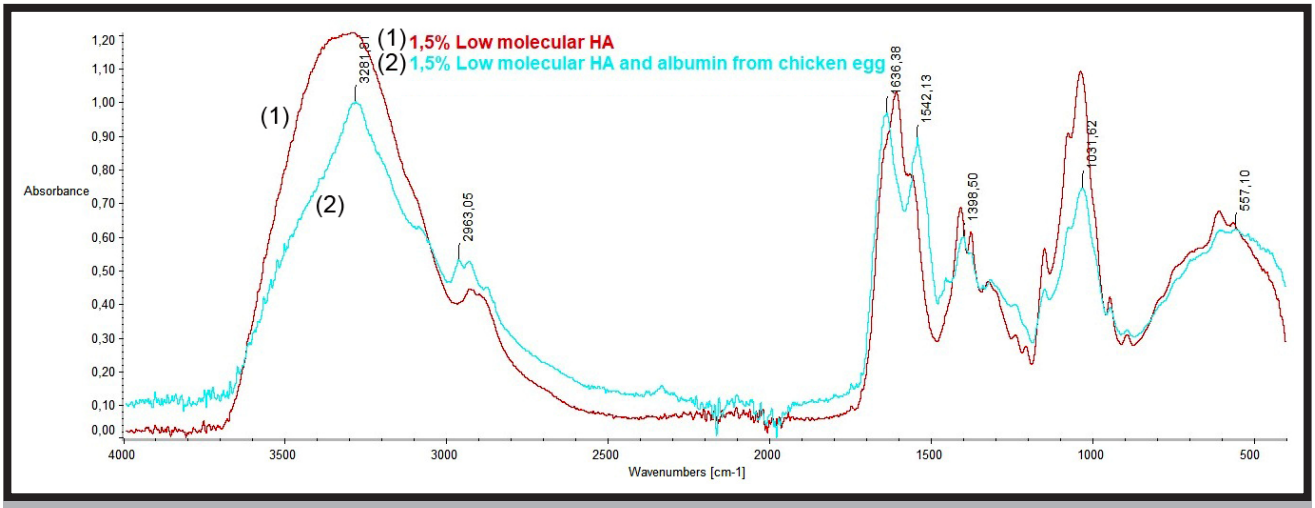

FIG. 7. The IR spectrum of the mixture of the 1.5% HA low molecular weight HA with albumin and the IR spectrum of pure low molecular weight HA.

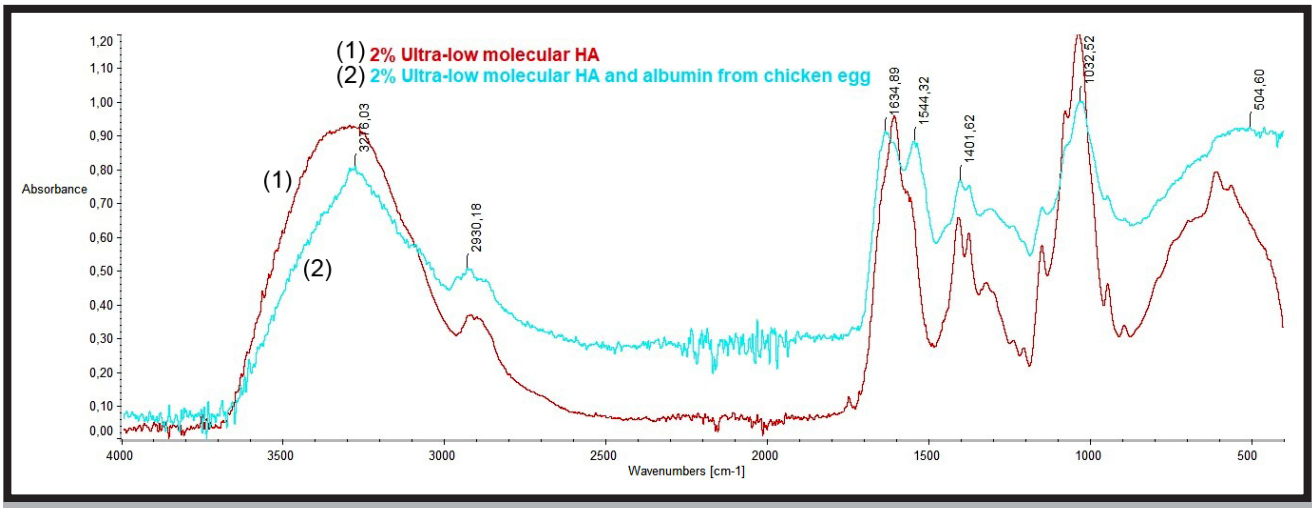

FIG. 8. The IR spectrum of the mixture of 2% HA of ultra-low molecular weight with albumin and the IR spectrum of the pure ultra-low molecular weight HA.

TABLE 1. Wavenumbers in IR spectra for bonds occurring in the high molecular weight hyaluronic acid and its mixture with egg albumin.

No.	Function group	Vibrations	Band position for hyaluronic acid [cm^{-1}]	Band position for the mixture of hyaluronic acid and albumin [cm^{-1}]
1	O-H; N-H	Stretching	3332	3287
2	C-H	Stretching	2928	2929
3	N-H	Deformative	1607	1635
4	C-N; N-H	Stretching; Bending	-	1543
5	C=O	Stretching	1409	1404
6	C=O	Stretching	1376	-
7	COH	Stretching	1038	1035
8	COC	Stretching	946	-
9	COC	Stretching	609	607

TABLE 2. Wavenumbers for bonds occurring in the low molecular weight hyaluronic acid and its mixture with egg albumin.

No.	Function group	Vibrations	Band position for hyaluronic acid [cm^{-1}]	Band position for the mixture of hyaluronic acid and albumin [cm^{-1}]
1	O-H; N-H	Stretching	3291	3281
2	C-H	Stretching	2927	2963
3	N-H	Deformative	1607	1636
4	C-N; N-H	Stretching; Bending	-	1542
5	C=O	Stretching	1408	1398
6	C=O	Stretching	1376	-
7	COH	Stretching	1036	1031
8	COC	Stretching	608	557

TABLE 3. Wavenumbers for bonds occurring in the ultra-low molecular weight hyaluronic acid and its mixture with egg albumin.

No.	Function group	Vibrations	Band position for hyaluronic acid [cm^{-1}]	Band position for the mixture of hyaluronic acid and albumin [cm^{-1}]
1	O-H; N-H	Stretching	3293	3276
2	C-H	Stretching	2919	2930
3	N-H	Deformative	1607	1634
4	C-N; N-H	Stretching; Bending	-	1544
5	C=O	Stretching	1408	1401
6	C=O	Stretching	1375	-
7	COH	Stretching	945	1032
8	COC	Stretching	606	504

The IR spectra for hyaluronic acid are almost identical, regardless of its molecular weight. Minor differences in the wavenumber may be caused by a slight change in conditions when performing spectrometric measurements. The obtained IR spectra confirm the presence of amide, hydroxyl, and carboxyl groups in the tested compounds.

The addition of egg albumin to hyaluronic acid changed the infrared spectra of this polysaccharide. The characteristic band for albumin, confirming the presence of protein in the tested film, is the band corresponding to the wavenumber 1543, 1542, and 1544 cm^{-1}. This band corresponds to the stretching of the C-N group and bending of the N-H group [23]. Reducing the intensity of the bands in mixtures and shift of the bands, e.g. 3332 cm^{-1} in HA and 3287 cm^{-1} in the mixture of HA with albumin, may suggest the interactions between the components of the mixtures. The interaction occurs mainly via hydrogen bonds.

The band of about 3300 cm^{-1} is attributed to vibrations stretching the OH bond and to vibrations stretching the NH bond, while the band of about 1600 cm^{-1} corresponds to deformation vibrations of the NH bond (presence of an amide functional group in the structure of hyaluronic acid). The band at 2930 cm^{-1} corresponds to the stretching vibration in the C-H group. The bands appearing around 1030 cm^{-1} and from 607 to 505 cm^{-1} may indicate stretching vibrations in the COC group. The C = O stretching vibration corresponds to the band around 1408-1375 cm^{-1} and confirms the presence of the carboxyl group in hyaluronic acid. The band appearing around 1038 cm^{-1} corresponds to the COH stretching vibrations [24,25]. Having added albumin to hyaluronic acid, the shift of the above-mentioned bands in the IR spectra clearly shows the interactions between the mixture components.

Mechanical properties

The mechanical properties of films made of pure hyaluronic acid solutions of three different molecular weights and of films produced by mixing hyaluronic acid with egg albumin were investigated. The obtained results are presented in the tables below (TABLES 4-6).

The mechanical properties of obtained polymeric films vary, depending on the molecular weight of the hyaluronic acid. The highest value of Fmax was obtained for the high-molecular weight HA, and the lowest for the ultra-low-molecular HA. The highest value of Young's modulus (Emod) was obtained for the ultra-low molecular weight HA.

The addition of ovalbumin to the hyaluronic acid solution significantly affects the mechanical properties of polymer films. The tested films made of mixtures of HA and albumin had lower Emod and Fmax values. The Fmax values for the mixtures decrease with the decreasing molecular weight of HA.

Changes in the mechanical properties following the addition of albumin may suggest interactions between hyaluronic acid and albumin. This has been confirmed in spectrometric tests. The weaker mechanical properties after the addition of egg albumin may suggest that the hydrogen bonds between HA and egg albumin are weaker than hydrogen bonds between HA molecules.

TABLE 4. Mechanical properties of the film made of the 1.5% high molecular weight hyaluronic acid solution and its mixture with egg albumin.

No.	Material	E_{mod} [GPa]	F_{max} [MPa]
1	HA	0.708	61.5
2	HA with albumin	0.298	48.07

TABLE 5. Mechanical properties of the film made of the 1.5% solution of low molecular weight hyaluronic acid and its mixture with egg albumin.

No.	Material	E_{mod} [GPa]	F_{max} [MPa]
1	HA	0.196	58.37
2	HA with albumin	0.220	38.02

TABLE 6. Mechanical properties of the film made of a 2% solution of ultra-low molecular weight hyaluronic acid and its mixture with egg albumin.

No.	Material	E_{mod} [GPa]	F_{max} [MPa]
1	HA	1.44	53.13
2	HA with albumin	0.303	17.85

Conclusions

Egg albumin can be combined with hyaluronic acid and thin films can be obtained. The addition of albumin reduces the mechanical properties of the hyaluronic acid films. The tensile strength of the HA films decreases when albumin is added to hyaluronic acid. This may be due to the interaction of albumin and hyaluronic acid and the formation of bonds weaker than those between HA molecules. The spectrometric studies confirmed the interactions between the hyaluronic acid molecule and albumin. The obtained polymer films based on hyaluronic acid and their mixtures with albumin can be used in the biomaterials and cosmetics industry, e.g. as biomimetic coatings and adhesives. The blends of hyaluronic acid and albumin can also be used in drug delivery systems. However, more research is needed to investigate the biological activity as well as the cosmetic and biomaterial potential of albumin-containing hyaluronic membranes. Nevertheless, it should be emphasized that the obtained biomaterial should be biocompatible and biodegradable as no cross-linking agent has been used for the materials preparation and the thin films were formed spontaneously via self-assembly.

Acknowledgements

Statutory activity of KCBiK WCh UMK in Toruń.

ORCID iDs

M. Gadomska: https://orcid.org/0000-0001-9214-8931
K. Musiał: https://orcid.org/0000-0002-3596-602X
A. Sionkowska: https://orcid.org/0000-0002-1551-2725

References

[1] Tyan Y.C., Yang M.H., Chang C.C., Chung T.W.: Biocompatibility of Materials for Biomedical Engineering. Advances in Experimental Medicine and Biology book series 1250 (2020) 125-140.

[2] Joyce K., Fabr, G.T., Bozkurt Y.: Bioactive potential of natural biomaterials: identification, retention and assessment of biological properties. Signal Transduction and Targeted Therapy 6 (2021) 122.

[3] Sionkowska A.: Current research on the blends of natural and synthetic polymers: Review. Progress in Polymer Science 36 (2011) 1254-1276.

[4] Werkmeister J.A., Edwards G.A., Casagranda F., White J.F., Ramshaw J.A.M.: Evaluation of a collagen-based biosynthetic materials for the repair of abdominal wall defects. Journal of Biomedical Materials Research 39 (1998) 429-36.

[5] Muthuraj R., Misra M., Mohanty A.K.: Biodegradable compatibilized polymer blends for packaging applications: A literature review. Journal of Applied Polymer Science 135 (2018) 45726.

[6] Younas M., Noreen A., Sharif A., Majeed A., Hassan A., Tabasum S., Mohammadi A., Zia K.M.: A review on versatile applications of blends and composites of CNC with natural and synthetic polymers with mathematical modelling. International Journal of Biological Macromolecules 124 (2019) 591-626.

[7] Tabasum S., Younas M., Zaeem M.A., Majeed I., Majeed M., Noreen A., Iqbal M.N., Zia K.M.: A review on blending of corn starch with natural and synthetic polymers, and inorganic nanoparticles with mathematical modelling. International Journal of Biological Macromolecules 122 (2019) 969-996.

[8] Tabasum S., Noreen A., Maqsood M.F., Umar H., Akram N., Nazli Z.I.H., Chatha S.A.S., Zia K.M. A review on versatile applications of blends and composites of pullulan with natural and synthetic polymers. International Journal of Biological Macromolecules 120 (2018) 603-32.

[9] Heidenreich A.C., Perez-Recalde M., Wusener A.G., Hermida E.B.: Collagen and chitosan blends for 3D bioprinting: A rheological and printability approach. Polymer Testing 82 (2020) 106297.

[10] Jurak M., Wiącek A.E., Ładniak A., Przykaza K., Szafran K.: What affects the biocompatibility of polymers?. Advances in Colloid and Interface Science 294 (2021) 102451.

[11] Xia G.X., Wu Y.M., Bi Y.F. et al.: Antimicrobial Properties and Application of Polysaccharides and Their Derivatives. Chinese Journal of Polymer Science 39 (2021) 133–146.

[12] Bealer E.J., Kavetsky K., Dutko S., Lofland S., Hu X.: Protein and Polysaccharide-Based Magnetic Composite Materials for Medical Applications. International Journal of Molecular Sciences 21 (2020) 186.

[13] Wang H., Deng H., Gao M., Zhang W.: Self-Assembled Nanogels Based on Ionic Gelation of Natural Polysaccharides for Drug Delivery. Frontiers in Bioengineering and Biotechnology 9 (2021) 703559.

[14] Vieira S., Strymecka P., Stanaszek L., Silva-Correia J., Drela K., Fiedorowicz M. Malysz-Cymborska I., Rogujski P., Janowski M., Reis R.L., Lukomska B., Walczak P., Oliveira J.M.: Methacrylated gellan gum and hyaluronic acid hydrogel blends for image-guided neurointerventions. Journal of Materials Chemistry B 8 (2020) 5928-5937.

[15] Ronca A., D'Amora U., Raucci M.G., Lin H., Fan Y.J., Zhang X.D., Ambrosio L.: A Combined Approach of Double Network Hydrogel and Nanocomposites Based on Hyaluronic Acid and Poly(ethylene glycol) Diacrylate Blend. Materials 11 (2018) 2454.

[16] Pokorny M., Rassushin V., Wolfova L., Velebny V.: Increased Production of Nanofibrous Materials by Electroblowing From Blends of Hyaluronic Acid and Polyethylene Oxide. Polymer Engineering and Science 56 (2016) 932-938.

[17] Chung E.J., Jakus A.E., Shah R.N.: In situ forming collagen--hyaluronic acid membrane structures: Mechanism of self-assembly and applications in regenerative medicine. Acta Biomaterialia 9 (2013) 5153-5161.

[18] Taguchi T., Ikoma T., Tanaka J.: An improved method to prepare hyaluronic acid and type II collagen composite matrices. Journal of biomedical materials research 61 (2002) 330-336.

[19] Park S.N., Lee H.J., Lee K.H., Suh H.: Biological characterization of EDC-crosslinked collagen-hyaluronic acid matrix in dermal tissue restoration. Biomaterials 24 (2003) 1631-1641.

[20] Lin Y.K., Liu D.C.: Studies of novel hyaluronic acid-collagen sponge materials composed of two different species of type I collagen. Journal of Biomaterials Applications 21 (2007) 265-281.

[21] Hu X., Ricci S., Naranjo S., Hill Z., Gawason Z.: Protein and Polysaccharide-Based Electroactive and Conductive Materials for Biomedical Applications. Molecules 26 (2021) 4499.

[22] Dong X., Zhang Y.Q.: An insight on egg white: From most common functional food to biomaterial application. Journal of Biomedical Materials Research 109 (2021) 1045-1058.

[23] Mahobia S., Bajpai J., Bajpai A.K.: An In-vitro Investigation of Swelling Controlled Delivery of Insulin from Egg Albumin Nanocarriers. Iranian Journal of Pharmaceutical Research 15 (2016) 695-711.

[24] OliveIra S.A., Silva B.C., Riegel-Vidotti I.C., Urbadno A., Sousa-Faria Tischer P.C.,Tischer C.A.: Production and characterization of bacterial cellulose membranes with hyaluronic acid from chicken comb. International Journal of Biological Macromolecules 97 (2017) 642-653.

[25] Hamad G.M., Taha T.H., Hafez E.E., Sohaimy S.: Physicochemical, Molecular and Functional Characteristics of Hyaluronic Acid as a Functional Food. American Journal of Food Technology 12 (2017) 72-85.

ASSESSMENT OF THE MICROSTRUCTURE AND MECHANICAL PROPERTIES OF POROUS GELATIN SCAFFOLDS

Anna Morawska-Chochół*

AGH University of Science and Technology,
Faculty of Materials Science and Ceramics,
Department of Biomaterials and Composites,
Al. A. Mickiewicza 30, 30-059 Krakow, Poland
*e-mail: morawska@agh.edu.pl

Abstract

Gelatin scaffolds are in the interest of tissue engineering and drug release. The scaffold porosity and microarchitecture are of great importance in proper tissue regeneration. In this work, the freeze-drying method was used to produce the scaffolds. The effect of concentration of the initial gelatin solution and pre-freezing temperature on the scaffold's microstructure and microarchitecture (porosity, pores size, shape, and distribution) was evaluated. The mechanical tests of samples were performed. Moreover, the influence of the gentamicin sulphate addition on the gelatin scaffolds microstructure and mechanical properties was also studied.

The linear relationship of porosity to the concentration of the initial solution was observed. Therefore, it is possible to obtain a scaffold with a planned porosity. Pores were interconnected with an aspect ratio between 1.5-1.8. For porosity 74 ± 9% the average pore size was 0.7 ± 0.6 mm, with most pores in the range 0.2-0.4 mm. For the samples with porosity 57 ± 14%, the average pore size was 0.2 ± 0.2 mm, with most pores in the range 0.05-0.2 mm. The process of pre-freezing the solution in liquid nitrogen caused the highest porosity of the sample, the smaller pores size and the lower pores size distribution in comparison to the sample pre-frozen in -20°C. The mechanical parameters for all the samples are sufficient for filling bone defects. The addition of a drug to gelatin caused only slight changes in the pore architecture. This material could be applied as a scaffold in the bone loss correlated to bacterial infection.

Keywords: *scaffold, microstructure, tissue engineering, gelatin, freeze-drying*

[Engineering of Biomaterials 160 (2021) 22-27]

doi:10.34821/eng.biomat.160.2021.22-27

Introduction

Porous scaffolds used in tissue engineering are fraught with many challenges. Designing biomaterials that meet the scaffolds requirements is very difficult. Choosing a proper method of scaffold production and designing its parameters is one of the key aspects affecting the final product [1-3]. The most popular techniques to fabricate gelatin scaffolds are electrospinning, phase separation, porogen leaching and self-assembly. Depending on the production method, properties, such as microstructure and mechanical strength may be modified. The lowest mechanical parameters are characteristic for woven biomaterials obtained in the electrospinning process. An extremely promising method of manufacturing porous substrates is the freeze-drying [4-6]. It avoids problems related to a solvent residue in the biomaterial and the use of high temperatures. Moreover, this method allows for introducing drugs or biological active agents to the scaffold [7].

The scaffold porosity and microarchitecture (pore size and shape, pore size distribution, pore connectivity) is of great importance in the cells adhesion and proliferation and in the proper tissue regeneration [8-10]. The trabecular bone porosity is about 60%. The largest frequency of pore size is in the range from 200 μm to 300 μm. The most optimal scaffold microarchitecture for trabecular bone regeneration is the porosity of about 60% and the pore size from 300 μm to 500 μm [11,12]. The choice of the method of scaffold manufacturing and also the selection of process parameters, such as the type and concentration of the solvent, the type and share of additives, temperature, allows to shape the microstructure for specific tissues. The porosity and the pores size have a big impact on the mechanical properties of scaffolds [12,13]. The high porosity and the presence of large pores negatively affect mechanical strength. Therefore, finding a compromise between the required porosity and the strength of scaffold plays a huge role in the design of porous substrates used in tissue engineering [8].

Gelatin is widely used in tissue engineering of bone, skin, cartilage and kidney [1,10,14,15]. It is a natural biopolymer derived from collagen hydrolysis. Gelatin scaffolds are biocompatible and polyampholyte, therefore they can induce the regeneration of tissue and organs. Moreover, this biopolymer may be modified by calcium phosphate ceramics or blended with synthetic polymers to improve mechanical properties and osteointegration [16]. Gelatin is also useful for controlled drug delivery. Most often, gelatin crosslinking is applied to slower drug release from samples [17]. Bacterial infections of bone tissue are a common problem after surgical operations and the inflammations result in bone defects. The most common drug used for bone healing is gentamicin sulphate [18]. Therefore, this study focuses on the possibility of gentamicin sulphate incorporation to the gelatin scaffold.

The aim of this work was to evaluate how the concentration of the initial gelatin solution influenced the microstructure of scaffolds obtained via a freeze-drying method. In this study, the freeze-drying method was selected due to the low temperature which allows for incorporation of biological substances to the scaffold (protein, drug).

Moreover, such a method does not require any additional substances such as porogen or solvent. The effect of pre-freezing temperature was also assessed. The scaffolds porosity, pores size, shape and distribution were analysed. The influence of the samples microstructure on their mechanical properties was also investigated. It was tested how gentamicin sulphate added to the gelatin solution affected the microstructure and pore microarchitecture. The gentamicin sulphate addition to the non-cross-linked gelatin structure was aimed to fasten the drug activity in the cases of bone losses often correlated to bacterial infection.

Materials and Methods

Sample preparation

Porous gelatin scaffolds were obtained by the freeze-drying method. Gelatin powder (bovine skin, type B, Sigma-Aldrich, bulk density 0.58 g/cm^3) was dissolved in distilled water in 3 different concentrations: **Sample 1** Cp = 11 wt%; **Sample 2** Cp = 14 wt%; **Sample 3** Cp = 20 wt%. The solutions were well mixed and then poured into a cell culture plate. 4 samples were obtained from each solution with the appropriate concentration. In the next step, they were placed in a freezer at about -20°C for 20 min. For comparison, one group of samples were frozen in liquid nitrogen (**Sample 1",** Cp = 11 wt%). Next, they were freeze-dried (Labconco freeze dryer). The process temperature was -60°C, the pressure was -0.09 mBar. The obtained samples were shaped as cylinders with a diameter of 12 mm and a length of 10 mm (FIG. 1). In the analogous way **Sample 4** with gentamicin sulphate (GS) was obtained. GS distributed in a small amount of water was added to the gelatin solution to obtain the final proportion of gelatin to water Cp = 11 wt%, and GS to gelatin 1 wt%.

Microstructure

The microstructure of scaffolds was assessed using a ZEISS stereoscopic microscope (StereoMicroscope, Zeiss). Porosity was determined using the point method as a probability of hit to the analyzed phase of point thrown randomly to the surface. The tests were performed using a 100-point grid (10 x 10) put to the surface 22 times. The average pore size D was calculated in a formula (1) where D1 is a longer diameter and D2 is a shorter diameter of pores. The aspect ratio K was calculated in the formula (2).

$$D = (D1+D2)/2 \quad (1)$$

$$K = D1/D2 \quad (2)$$

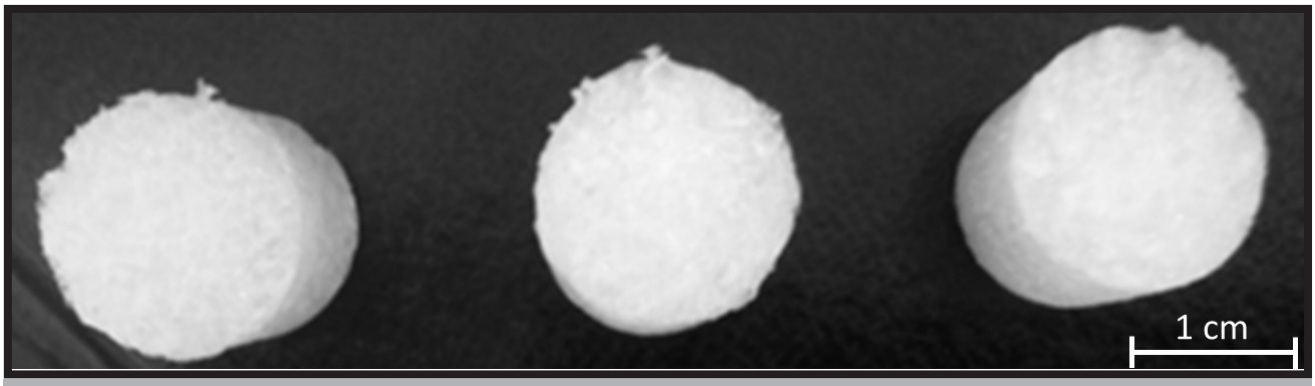

FIG. 1. Shape of the samples.

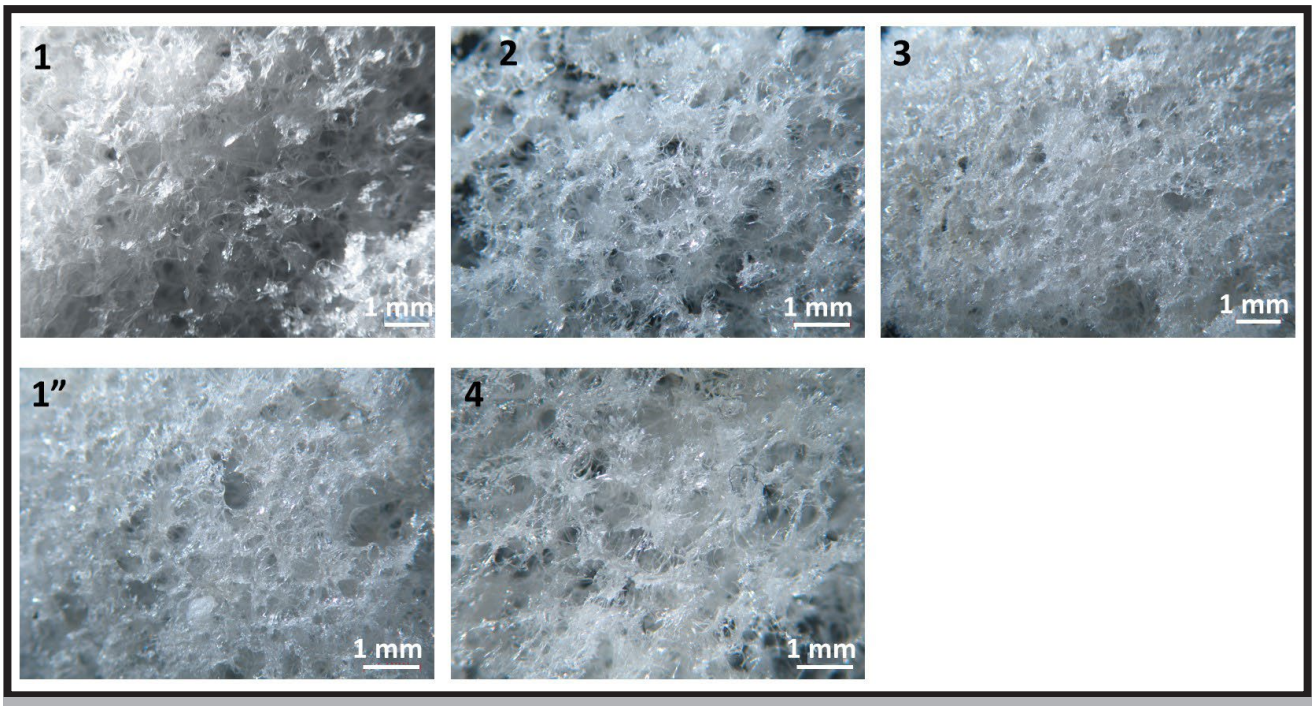

FIG. 2. SEM micrograph of the Samples 1 - 4 and 1".

Mechanical tests

Mechanical properties were measured in a compressive test by using a universal testing machine (Zwick 1435). The compression speed was 2 mm/min. The test was finished when the displacement reached 5 mm.

Statistical analysis

The statistical analysis was performed with Student's t-test (with confidence level 0.95). The data were expressed as the mean ± standard deviation.

Results and Discussion

FIG. 2 shows the microstructure of the obtained scaffolds. All the samples have irregular, connected pores. It is an important feature regarding tissue engineering as it allows for cells migration, and for the transport of the biological active agents. The pores sizes and aspect ratio of pores for all the samples are presented in TABLE 1. The measured values of the longer and the shorter diameter of pores confirm their irregular, elongated shape. This is also indicated by the aspect ratio, which is appr. between 1.6-1.8. It is also clearly visible that the average pores size is strongly influenced by the concentration of initial solutions. The largest average pore size is observed for Sample 1 (0.747 mm), for Sample 2 the pore size is equal to about 0.318 mm, and for Sample 3 the smallest pore size is measured (0.229 mm). The histograms show the larger dispersion of average pore size for Sample 1 (FIG. 3). The most pores are in the range of 0.2-0.4 mm, but there are also pores above 1 mm in size. Sample 2 contains less varied pores. The most pores are in the range of 0.2-0.3 mm, however, the large frequency of pore size is also in the range from 0.075-0.5 mm. For Sample 3 the small dispersion of pore size is visible, and the most pores are in the size range of 0.05-0.2 mm. The largest pores are present only individually. The characteristic of obtained scaffolds is similar to the microstructure of natural tissue, especially to bone tissue [8].

The analysis of the microstructure of obtained scaffolds shows that porosity is highly dependent on polymer concentration. The real and theoretical porosity of scaffolds are presented in TABLE 2. The theoretical porosity was calculated from the volume ratio of water used for preparing the gelatin solution. The measured porosity or Samples 1, 2 and 3 is appropriately: 74, 68, 57%. As assumed, the lowest concentration of polymer (Sample 1) has the highest porosity, and the highest concentration of polymer (Sample 3) has the lowest porosity. What is important, there are no statistically significant differences between the theoretical and the measured porosity. A large standard deviation of porosity is visible. It results from the high variation in pore size and the uneven distribution of pores in the structure of the scaffolds. The linear relationship of porosity to the concentration of the initial solution allows to determine what concentration should be used to obtain a scaffold with the planned porosity (FIG. 4).

TABLE 1. Pore size and shape of the samples.

Pore size and shape	Longer diameter D1 [mm]	Shorter diameter D2 [mm]	Average pore size D [mm]	Aspect ratio K
Sample 1	0.940 ± 0.778	0.554 ± 0.428	0.747 ± 0.595	1.744 ± 0.404
Sample 2	0.381 ± 0.251	0.254 ± 0.152	0.318 ± 0.198	1.493 ± 0.308
Sample 3	0.293 ± 0.277	0.179 ± 0.144	0.229 ± 0.204	1.661 ± 0.542
Sample 1"	0.342 ± 0.259	0.228 ± 0.148	0.293 ± 0.158	1.552 ± 0.249
Sample 4	0.872 ± 0.522	0.487 ± 0.334	0.652 ± 0.455	1.79 ± 0.401

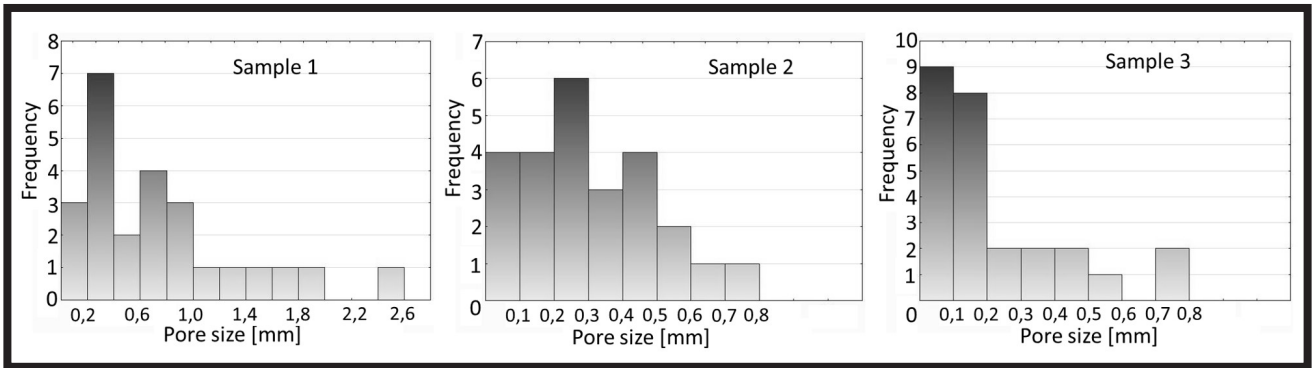

FIG. 3. Frequency of the pore size in a particular range for samples 1, 2 and 3.

TABLE 2. Porosity of the obtained samples in comparison with theoretical values.

	Sample 1	Sample 2	Sample 3	Sample 1"	Sample 4
Measured porosity [%]	74 ± 9	68 ± 11	57 ± 14	78 ± 5	73 ± 10
Theoretical porosity [%]	82	78	70	82	82

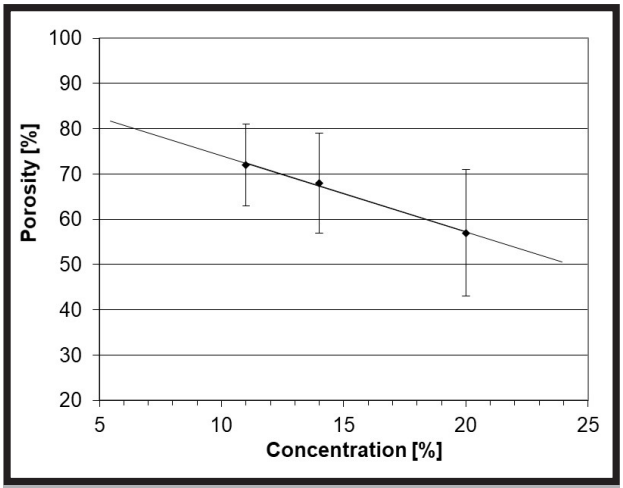

FIG. 4. The relation of porosity from the concentration of initial gelatin solution.

For comparison, the results for Sample 1" frozen in liquid nitrogen before freeze-drying are presented. In this case the pores are significantly smaller than for Sample 1 (average pore size for Sample 1" is 0.293 ± 0.158 mm and for sample 1 is 0.747 ± 0.595 mm). Moreover, the standard deviation is also lower, and it indicates that the pores size is less diverse. The porosity of Sample 1" is more adequate to theoretical value than for Sample 1. The largest frequency of pore size is in the range from 0.1 mm to 0.3 mm (FIG. 5). This manner of sample preparation i.e. freezing in liquid nitrogen can be used when the scaffold should be applied for smaller cells than bone cells.

The addition of the drug to gelatin scaffold caused a slight reduction in the size of pores, however, the changes are in the error range (TABLE 1). The histogram of Sample 4 is also different when compared to Sample 1 (FIG. 5). Dispersion of results is lower, the most pores are in the range 0.2-0.3 mm, however the high frequency of pore size is also in the range 0.1-0.7 mm. The total porosity of Sample 4 is not changed (TABLE 2).

The mechanical parameters of the obtained samples were investigated in the compression test (TABLE 3). This study shows a close dependence of mechanical parameters on the porosity of the samples. The lowest Young's modulus is observed for Sample 1 with the highest porosity. Moreover, in this case, the lowest force is required (103 N) to cause a 10% deformation. For comparison, such a deformation of Sample 3 requires a force of 156 N. The compression stress at 50% strain was also evaluated, and the values for all the samples equalled 3.01-3.4 MPa. The highest value of this parameter (3.4 MPa) was observed for Sample 3 characterized by the lowest porosity. The measured forces are sufficient for the resulting substrates to act as a scaffold for bone tissue regeneration [19-21]. Scaffolds obtained from natural polymers are usually characterized by poor mechanical properties, and the compression strength very often does not exceed 1 MPa [22]. Apart from total porosity, the shape and orientation of pores also affect the mechanical properties of scaffolds. Arora et al. reported maximum mechanical properties for aligned pores [23]. Vetrik et al. observed the greater compressive strength for more complex morphological architecture [24]. Roosa et al. described that the matching the pore size to the cell dimension provided better mechanical strength after implantation due to the initial pores filling with cells [25].

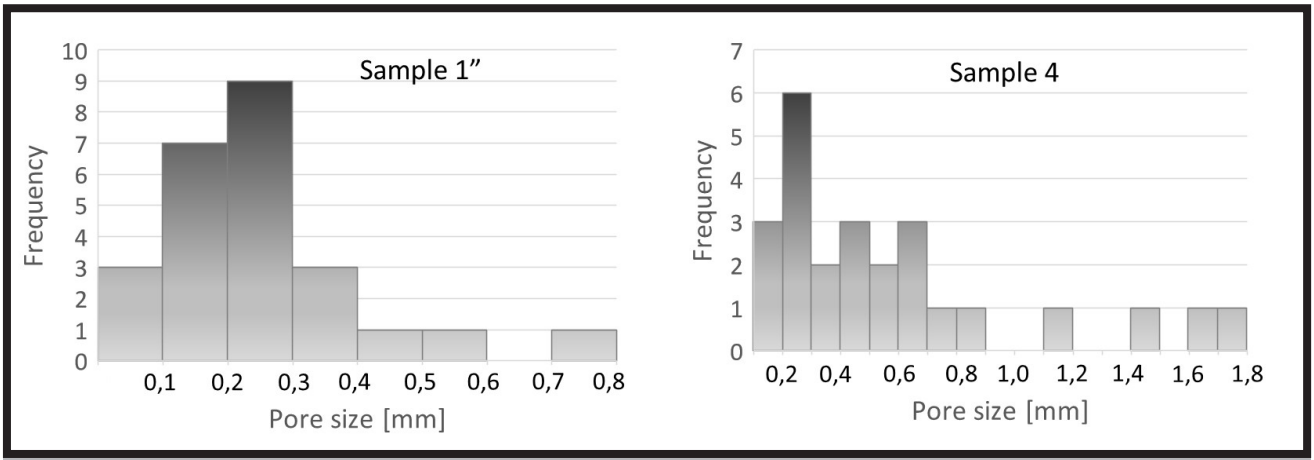

FIG. 5. Frequency of pore size in particular range for Samples 1" and 4.

TABLE 3. Mechanical properties of scaffolds.

	Sample 1	Sample 2	Sample 3	Sample 1"	Sample 4
Young's modulus E [GPa]	0.05 ± 0.01	0.06 ± 0.01	0.07 ± 0.01	0.06 ± 0.01	0.08 ± 0.01
Compression strength $\sigma_{(\varepsilon = 50\%)}$ [MPa]	3.01 ± 0.15	3.16 ± 0.42	3.40 ± 0.39	3.13 ± 0.17	3.09 ± 0.20
Force at 10% strain [N]	103 ± 4	123 ± 10	156 ± 6	121 ± 5	115 ± 7

Sample 1" which was obtained by pre-freezing in liquid nitride is characterized by higher mechanical properties when compared with Sample 1. It can be related with the presence of smaller pores in the microstructure and their more homogenous distribution. Moreover, the addition of gentamicin sulphate also improves the mechanical properties. In this case, the force causing 10% deformation is higher as compared to Sample 1, moreover elasticity of Sample 4 is lower. This is important during the initial stage after implantation. However, as gelatin is no crosslinked, the rapid drug release and fast gelatin degradation can be expected, and in consequence the fast mechanical parameters decrease. In this stage of the study, a rapid antibacterial action of the scaffold was planned.

Conclusions

Freeze-drying is a very useful method for manufacturing scaffolds with additives (e.g. drug) for tissue regeneration. Changing the initial polymer solution and pre-freezing of the samples makes it possible to create the desired microstructure and to precisely control the microstructure parameters. The linear relationship of porosity to the concentration of the initial solution is observed. Such a dependence allows to determine what concentration should be used to obtain a scaffold with planned porosity. For all the samples, the pores are interconnected, with longitudinal shape, aspect ratio between 1.5-1.8.

The lower initial gelatin solution concentration caused higher porosity (74 ± 9%) and the bigger pores size (average pore size 0.7 ± 0.6 mm, most pores in the range 0.2-0.4 mm). For the samples with a higher solution concentration porosity was 57 ± 14%, with an average pore size 0.2 ± 0.2 mm and most pores in the range 0.05-0.2 mm.

The pre-freezing of the solution in liquid nitrogen caused the highest porosity of sample, the smaller pores size and the smaller pores size distribution in comparison to the sample pre-frozen in -20°C.

The obtained samples microstructure (especially for Sample 1) is adequate for bone tissue regeneration. The mechanical parameters for all the samples are sufficient for this application.

The addition of drug to gelatin caused only slight changes in the pore architecture, and the observed changes were within the error margin. However, the addition of gentamicin sulphate improved the mechanical properties of the scaffolds.

The next step of the studies will be investigating a drug release profile and assessing the influence of gelatin crosslinking on the drug release speed.

Acknowledgement

This work was supported from the subsidy of the Ministry of Education and Science for the AGH University of Science and Technology in Kraków (Project No 16.16.160.557).

MSc Joanna Herman is gratefully acknowledged for data acquisition and initial graphics preparation.

ORCID iDs

A. Morawska-Chochół: https://orcid.org/0000-0003-0209-4402

References

[1] Bello A.B., Kim D., Kim D., Park H., Lee S.H.: Engineering and functionalization of gelatin biomaterials: from cell culture to medical applications. Tissue Engineering - Part B Reviews 26 (2) (2020) 164-180.

[2] Meng C., Su W., Liu M., Yao S., Ding Q., Yu K., Xiong Z., Chen K., Guo X., Bo L. et al.: Controlled delivery of bone morphogenic protein-2-related peptide from mineralised extracellular matrix--based scaffold induces bone regeneration. Materials Science and Engineering C 126 (2021) 112182.

[3] Li J., You F., Li Y., Zuo Y., Li L., Jiang J., Qu Y., Lu M., Man Y., Zou Q.: Bone regeneration and infiltration of an anisotropic composite scaffold: An experimental study of rabbit cranial defect repair. Journal of Biomaterials Science: Polymer Edition 27 (4) (2016) 327-338.

[4] Domalik-Pyzik P., Morawska-Chochół A., Chłopek J., Rajzer I., Wrona A., Menaszek E., Ambroziak M.: Polylactide/polycaprolactone asymmetric membranes for guided bone regeneration. E-Polymers, 16 (5) (2016) 351-358.

[5] Fereshteh Z.: Freeze-drying technologies for 3D scaffold engineering. In Functional 3D Tissue Engineering Scaffolds: Materials, Technologies, and Applications; Woodhead Publishing, 2018, 151-174.

[6] Kulikouskaya V.I., Lazouskaya M.: Fabrication and physicochemical properties of pectin/chitosan scaffolds (Engineering of Biomaterials 146 (2018) 2-7.

[7] Kazimierczak P., Vivcharenko V., Truszkiewicz W., Wójcik M., Przekora A.: Osteoblasts response to novel chitosan/agarose/hydroxyapatite bone scaffold – studies on MC3T3-E1 and HFOB 1.19 cellular models. Engineering of Biomaterials 151 (2019) 24-29.

[8] Abbasi N., Hamlet S., Love R.M., Nguyen N.T.: Porous scaffolds for bone regeneration. Journal of Science: Advanced Materials and Devices 5 (1) (2020) 1-9.

[9] Mullick P., Das G., Aiyagari R.: Probiotic bacteria cell surface--associated protein mineralized hydroxyapatite incorporated in porous scaffold: In vitro evaluation for bone cell growth and differentiation. Materials Science and Engineering C 126 (2021) 112101.

[10] Maji K., Dasgupta S., Pramanik K., Bissoyi A.: Preparation and evaluation of gelatin-chitosan-nanobioglass 3D porous scaffold for bone tissue engineering. International Journal of Biomaterials 2016 (2016) Article ID 9825659.

[11] Doktor T., Valach J., Kytyr D., Jirousek O.: Pore size distribution of human trabecular bone - comparison of intrusion measurements with image analysis. In 17th International Conference Engineering Mechanics 2011, Svratka, Czech Republic, 9-12 May 2011 (2011) 115-118.

[12] Torres-Sanchez C., Al Mushref F.R.A., Norrito M., Yendall K., Liu Y., Conway P.P.: The effect of pore size and porosity on mechanical properties and biological response of porous titanium scaffolds. Materials Science and Engineering C 77 (2017) 219-228.

[13] Aoki K., Haniu H., Kim Y.A., Saito N.: The use of electrospun organic and carbon nanofibers in bone regeneration. Nanomaterials 10 (3) (2020) 562.

[14] Hoque M.E., Nuge T., Tshai K.Y., Nordin N., Prasad V.: Gelatin based scaffolds for tissue engineering – A review. Polymer Reaearch Journal 9 (1) (2015) 15-32.

[15] Echave M.C., Hernáez-Moya R., Iturriaga L., Pedraz J.L., Lakshminarayanan R., Dolatshahi-Pirouz A., Taebnia N., Orive G.: Recent advances in gelatin-based therapeutics. Expert Opinion on Biological Therapy 19 (8) (2019) 773-779.

[16] Samadian H., Farzamfar S., Vaez A., Ehterami A., Bit A., Alam M., Goodarzi A., Darya G., Salehi M.: A tailored polylactic acid/polycaprolactone biodegradable and bioactive 3D porous scaffold containing gelatin nanofibers and taurine for bone regeneration. Scientific Reports 10 (1) (2020) 1-12.

[17] Laha A., Bhutani U., Mitra K., Majumdar S.: Fast and slow release: synthesis of gelatin casted-film based drug delivery system. Materials and Manufacturing Processes 31 (2) (2016) 223-230.

[18] Morawska-Chochół A., Chłopek J., Szaraniec B., Domalik--Pyzik P., Balacha E., Boguń M., Kucharski R.: Influence of the intramedullary nail preparation method on nail's mechanical properties and degradation rate. Materials Science and Engineering C 51 (2015) 99-106.

[19] Khairol Anuar Mohd Ariffin M., Hajar Fazel S., Idris Shah Ismail M., Mohamed S.B., Wahid Z.: Mechanical properties of bone scaffold prototypes fabricated by 3D printer. Journal of Engineering Science and Technology 13 (2018) 29-38.

[20] Qu H., Fu H., Han Z., Sun Y.: Biomaterials for bone tissue engineering scaffolds: a review. RSC Advances 9 (2019) 26252-26262.

[21] Hunger M., Domalik-Pyzik P., Reczyńska K., Chłopek J.: Double crosslinking of chitosan/vanillin hydrogels as a basis for mechanically strong gradient scaffolds for tissue engineering. Engineering of Biomaterials 155 (2020) 2-11.

[22] Grover C.N., Cameron R.E., Best S.M.: Investigating the morphological, mechanical and degradation properties of scaffolds comprising collagen, gelatin and elastin for use in soft tissue engineering. Journal of the Mechanical Behaviour of Biomedical Materials10 (2012) 62-74.

[23] Arora A., Kothari A., Katti D.S.: Pore Orientation Mediated Control of Mechanical Behavior of Scaffolds and Its Application in Cartilage-Mimetic Scaffold Design. Journal of the Mechanical Behavior of Biomedical Materials 51 (2015) 169-183.

[24] Vetrik M., Parizek M., Hadraba D., Kukackova O., Brus J., Hlidkova H., Komankova L., Hodan J., Sedlacek O., Slouf M., et al.: Porous heat-treated polyacrylonitrile scaffolds for bone tissue engineering. ACS Applied Materials & Interfaces 10 (10) (2018) 8496-8506.

[25] Roosa S.M.M., Kemppainen J.M., Moffitt E.N., Krebsbach P.H., Hollister S.J.: The pore size of polycaprolactone scaffolds has limited influence on bone regeneration in an in vivo model. Journal of Biomedical Materials Research Part A 92A (1) (2010) 359-368.